Cretaceous Research 125 (2021) 104844

Contents lists available at ScienceDirect

Cretaceous Research

journal homepage: www.elsevier.com/locate/CretRes

Influence of the Latest Maastrichtian Warming Event on planktic foraminiferal assemblages and ocean carbonate saturation at Caravaca, Spain

Vicente Gilabert [a, *], José A. Arz [a], Ignacio Arenillas [a], Stuart A. Robinson [b], Daniel Ferrer [a]

[a] Departamento de Ciencias de La Tierra, and Instituto Universitario de Investigación en Ciencias Ambientales de Aragón, Universidad de Zaragoza, E-50009 Zaragoza, C/ Pedro Cerbuna 12, 50009 Zaragoza, Spain
[b] Department of Earth Sciences, University of Oxford, South Parks Road, Oxford, OX1 3AN, UK

ARTICLE INFO

Article history:
Received 26 May 2020
Received in revised form
16 February 2021
Accepted in revised form 31 March 2021
Available online 14 April 2021

Keywords:
Deccan volcanism
Stable isotopes
Mass extinction
Western Tethys

ABSTRACT

A global warming episode in the Late Cretaceous, the Latest Maastrichtian Warming Event (LMWE), has been commonly linked to both the onset of massive Deccan Trap volcanism and the start of a planktic foraminiferal mass extinction prior to the Cretaceous/Paleogene boundary (KPB). The mechanisms that drove the LMWE are still under discussion, but radiometric dating of the onset of the main phase of the Deccan volcanism supports a temporal coincidence and permits a potential mechanistic link. Here we evaluate the planktic foraminiferal record, carbonate content and stable carbon and oxygen isotopes in the Caravaca section, in order to characterize paleoenvironmental change related to the LMWE. We identified negative $\delta^{13}C$ and $\delta^{18}O$ excursions in bulk carbonate from 66.35 to 66.14 Ma, i.e. ~310 to ~100 kyr before the KPB, which can be stratigraphically correlated to the LMWE and a major pulse of Deccan Traps volcanism. Within this warm interval, we identified high values in the fragmentation index of planktic foraminiferal tests, episodes of very high abundance of the low oxygen tolerant genus *Heterohelix*, a decrease of thermocline dwellers, dwarfing in *Contusotruncana contusa* tests, and an increase in the biserial morphotype of *Pseudoguembelina hariaensis* with elongated terminal chambers. However, the environmental disturbance during the LMWE did not cause changes in the planktic foraminiferal extinction rate. At Caravaca, the warming associated with LMWE was followed by a gradual cooling up to the KPB suggesting no extended interval of perturbed environments before the KPB extinction due to Deccan volcanism.

1. Introduction

For more than 40 years there has been a debate about the tempo and causes of the end-Cretaceous mass extinction ~66 Ma ago, with the Chicxulub impact widely argued to be the major contributing factor (e.g., Alvarez et al., 1980; Hull et al., 2020; Kring, 2007; Schulte et al., 2010a; Smit, 1982). Nonetheless, more accurate magnetochronological studies (Chenet et al., 2007, 2009) and radiogenic isotope dating of rocks from the Deccan Traps in India (Chenet et al., 2008), have fueled the debate over whether there was a single cause, the Chicxulub impact (Schulte et al., 2010a,b), or a combination of causes, with uncertain relative contributions (Courtillot and Fluteau, 2010; Keller et al., 2010). Radiometric dating of intertrappean zircon crystals using the uranium-lead (U–Pb) geochronometer (Schoene et al., 2015, 2019), and new precise ages using $^{40}Ar/^{39}Ar$ geochronology, have proven that the Deccan megaflows erupted during almost 1 Ma, fully spanning the magnetochron C29r (Renne et al., 2015; Sprain et al., 2019) in which the Cretaceous/Paleogene boundary (KPB) event occurred. Planktic foraminiferal biostratigraphic studies in the intertrappean marine sediments from the Krishna-Godavari Basin, SE India, are consistent with an onset of the Deccan main eruptive phase near the C29r/C30n reversal (Keller et al., 2008, 2012).

A decline in the marine $^{187}Os/^{188}Os$ ratio (Robinson et al., 2009) provides the most unequivocal geochemical evidence for the timing in the marine sedimentary record of this latest Maastrichtian high-flux magma pulse. Although some authors have

* Corresponding author.
E-mail addresses: vgilabert@unizar.es (V. Gilabert), josearz@unizar.es (J.A. Arz), ias@unizar.es (I. Arenillas), stuart.robinson@earth.ox.ac.uk (S.A. Robinson), danielferrer26795@gmail.com (D. Ferrer).

https://doi.org/10.1016/j.cretres.2021.104844

suggested an increased input of volcanogenic Hg during the latest Maastrichtian (e.g., Sial et al., 2016; Font et al., 2016, Font et al., 2017) the patterns are not consistent between sites or through time (Percival et al., 2018), suggesting this proxy cannot be used as a reliable and consistent stratigraphic marker of Deccan volcanism. Alongside the geochemical evidence for volcanism, other records suggest that the carbonate system was perturbed during this time, possibly as a result of outgassing from the Deccan Traps (e.g. Kucera et al., 1997; Font et al., 2014; Punekar et al., 2014; Henehan et al., 2016; Keller et al., 2016; Dameron et al., 2017).

Global warming intervals during the KPB interval have been well documented from oxygen isotope ($\delta^{18}O$) records for several decades, and have been commonly related to increased emissions of carbon dioxide greenhouse gases from the Deccan Traps (Stott and Kennett, 1990; Li and Keller, 1998a; Barrera and Savin, 1999). The magnitude of the temperature increase during the well-known Latest Maastrichtian Warming Event (LMWE) has been estimated to have been between 5 and 8 °C in the terrestrial realm from localities in North America (Nordt et al., 2003; Wilf et al., 2003) and NE China (Zhang et al., 2018). In the marine realm, contemporaneous warming episodes have been recognized in the North Atlantic Ocean (3.9 ± 1.1 °C in the ODP 174AX Bass River core by Woelders et al., 2018); the South Atlantic Ocean (~2 to 5 °C at ODP 1262 and DSDP 525A Sites by Barnet et al., 2018; Li and Keller, 1998a); Pacific Ocean (~3 °C at ODP 1209 Site by Westerhold et al., 2011); and the Southern Ocean (7.8 ± 3.3 °C at Seymour Island by Petersen et al., 2016). Recently, Hull et al. (2020) have modelled several scenarios for the timing of outgassing from the Deccan Traps and the climatic effects of volcanic emissions of CO_2 and SO_2. Based on this modelling, Hull et al. (2020) suggest that the most likely scenario was one in which 50% of the degassing of the Deccan Traps occurred between 358 kyr (C29r/C30n reversal boundary) and 218 kyr before the KPB, with the other 50% of eruptive degassing events occurring in the early Danian.

Most of the evidence for the paleobiological response to the LMWE comes from marine records including, among others, blooms in the warm-water calcareous nannofossil *Micula murus* (Thibault et al., 2016), blooms of the planktic foraminiferal opportunist species *Guembelitria cretacea* (Punekar et al., 2014), blooms in *Palynodinium grallator* dinoflagellate cysts (Vellekoop et al., 2019) and changes in bivalve assemblages (Petersen et al., 2016). According to some authors (Wilf et al., 2003; Keller et al., 2008, 2016; Gertsch et al., 2011; Keller, 2014), the age constraints for the LMWE and the terrestrial and marine paleobiological and geochemical data suggest that the global climate change triggered by Deccan volcanism started the end-Cretaceous extinctions. However, others found no evidence of extinctions or significant changes in the community structure of marine microbiota during the LMWE (see extensive compilation in Table S1 of Hull et al., 2020), suggesting that the environmental and climatic effects of Deccan Trap volcanism alone were insufficient to drive biotic extinctions.

To of improve our knowledge about the role of the Deccan Traps in the complex paleoclimatic and paleobiological changes that took place during the latest Maastrichtian, we provide a detailed multiproxy analysis of the last ~400 kyr of the Maastrichtian at the Caravaca section (SE Spain, western Tethys), including quantitative, biometric and taphonomic studies of planktic foraminifera, as well as bulk geochemical measurements (stable C- and O-isotopes, $CaCO_3$ content). Several decades ago, the Caravaca section played a key role in testing the tempo and duration of biotic and environmental changes across the KPB (catastrophic vs gradual mass extinction; e.g. Smit, 1982 vs Canudo et al., 1991). However, most of the previous analyses performed at Caravaca have been focused only on the uppermost Maastrichtian rocks (~last meter), thereby failing to capture the environmental influence of the late Maastrichtian Deccan eruptive phase.

2. Geological settings

The Caravaca section is located in southern Spain (Murcia region), about 4 km south of the town of Caravaca, in the Barranco del Gredero ravine (38°04′36″ N, 1°52′42″ W). Geologically, the section lies in the Betic System (Subbetic Zone) which represents the westernmost edge of the Alpine Orogeny. Caravaca is one of the most complete, expanded, and well-exposed KPB outcrops in the world (Smit, 2004) and was designated as an auxiliary section for the Global Boundary Stratotype Section and Point (GSSP) for the base of the Danian Stage (Molina et al., 2009). On the basis of benthic foraminifera, Coccioni and Galeotti (1994) reported that the terminal Maastrichtian to basal Danian sedimentary rocks were deposited in an open marine middle-bathyal environment with a paleodepth of about 600–1000 m, similar to previous estimations of Smit (1982) (Fig. 1).

The uppermost Maastrichtian interval is defined as the Raspay Formation by Chacon (2002) and consists of 45 m of hemipelagic marlstones with some marly limestones intercalations. In this study, we focused only on the last 18.3 m immediately underlying the KPB since, from this level to downwards, the outcrop is no longer accessible.

The stratigraphic interval studied is thicker than that analyzed by Arz et al. (2000), which focused on the KPB mass extinction event, and consists mainly of limy marlstones and marly limestones (Fig. 2) rich in planktic foraminifera with rare, minor intercalations of siliciclastic turbidites. Lithologies have been distinguished on the basis of the $CaCO_3$ content with 75–95% for marly limestones, 65–75% for limy marlstones and 35–65% for marlstones. From base to top we differentiated five lithologic intervals: 1) 2.4 m of greyish marly limestones; 2) 5.8 m of whitish limy marlstones with some centimetric to decimetric marly limestones intercalations and some scarce millimetric to centimetric siliciclastic turbidites; 3) 3.6 m of a gradual succession of whitish marlstones, limy marlstones and marly limestones. 4) 4.7 m of a rhythmic alternation between whitish limy marlstones with greyish marly limestones 20–40 cm thick; 5) 1.8 m of massive greyish marlstones with some centimetric to millimetric limy marlstone intercalations that get thinner towards the top. The KPB at Caravaca is marked by a 2 to 3 mm-thick rusty red layer that contains altered microtektites (Smit and Klaver, 1981), as well as anomalously high concentrations of Ir, Co, Cr, Ni, As, Sb, and Se (Smit and Ten Kate, 1982).

3. Material and methods

3.1. Micropaleontological methods

Fifty-eight samples were carefully disaggregated in 10% diluted H_2O_2 for 2 h each, then washed and passed gently through 63, 100 and 1000 μm mesh sieves, and finally dried in an oven at less than 50 °C. For planktic foraminiferal biostratigraphy, age model and specific richness determinations, we carried out an intensive scanning of the residue to minimize the Signor-Lipps effect (Signor and Lipps, 1982), trying to identify all the scarce species present in the samples (see Table 1 in the supplementary data).

Later, a subset of 35 samples was selected for paleoenvironmental analysis, using an Otto microsplitter over the >63 μm size fraction to obtain a representative aliquot in each sample. We randomly picked about 500 whole planktic foraminifera tests per sample, and classified them at genus level in order to evaluate changes in the relative abundance of each genus. Changes in depth-habitat ecogroups were investigated using the deep-surface (D/S)

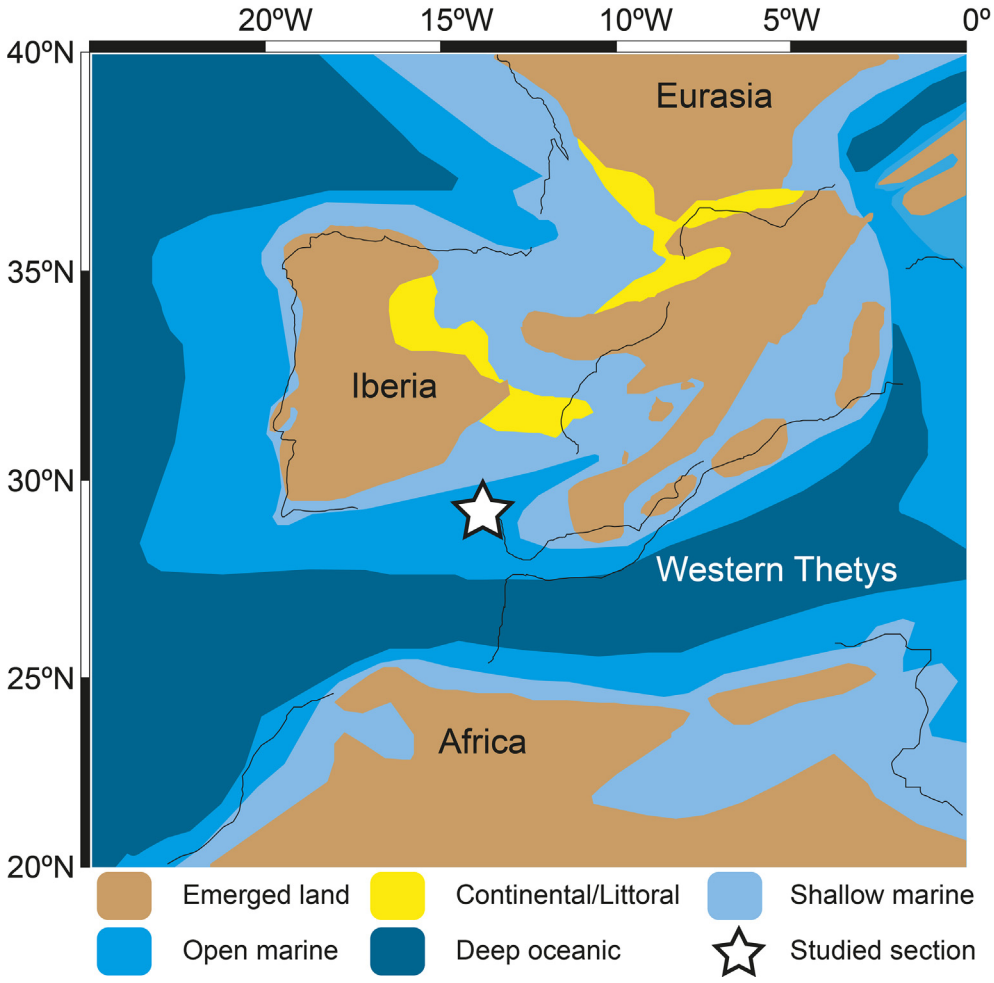

Fig. 1. Paleogeographic reconstruction of western Tethys, showing the position of the Caravaca section. Modified from ODSN Plate Tectonics Reconstruction Service and Andeweg (2002).

ratio, calculated as follows: D/S = [thermocline dwellers/(thermocline dwellers + mixed layer dwellers)]. It is used as a proxy to analyze the water column state, with higher values suggesting more stable conditions with a deeper and wider thermocline or an increase in the suitability of the upper water column for planktic foraminifera. Interpretations of depth-habitat ecogroups are based mainly on stable isotope signatures and paleoecological data of planktic foraminiferal species from D'Hondt and Zachos (1993), D'Hondt and Arthur (1995), Abramovich et al. (2003), Isaza-Londoño et al. (2006), Georgescu et al. (2008), Abramovich et al. (2010), 2011), Ashckenazi-Polivoda et al. (2014), Falzoni et al. (2014, 2016), Petrizzo et al. (2020). We have adopted the depth ecology categories of Petrizzo et al. (2020) which differentiate between mixed layer, intermediate and thermocline dwelling planktic foraminifera (Table 1). Finally, in order to quantify the planktic/benthic (P/B) ratio and estimate changes in the paleobathymetry, we have picked the benthic foraminiferal specimens in each sample over the same split as the 500 whole planktic foraminiferal tests. The P/B ratio was calculated as follow: P/B = [planktic foraminifera/(planktic + benthic foraminifera)] * 100.

For the taphonomic analysis, we additionally picked fragments of planktic foraminiferal tests over the same 35 sample set and >63 μm splits in order to identify episodes of enhanced fragmentation. Planktic foraminiferal test preservation is usually moderate to good (Fig. 3), but highly variable in some stratigraphic intervals (Fig. 4). The fragmentation index is a well-known taphonomic proxy of carbonate saturation state or dissolution of calcium carbonate (Berger et al., 1982; Malmgren, 1987), and it is considered a better proxy to quantify these variables than other indicators such as weight percent $CaCO_3$ or weight percent coarse fraction (Henehan et al., 2016). The fragmentation index (FI) measures the percentage of planktic foraminiferal fragments (specimens consisting of less than two-third on an entire test) in relation to the total number of whole tests, following Berger et al. (1982). We considered that the dissolution effects upon the composition of planktic foraminifera assemblages were substantially higher in samples with FI >40%. This boundary has been previously used to distinguish between regimes of moderate and strong dissolution in other upper Cretaceous sections (e.g., Malmgren, 1987; Kucera et al., 1997). The sample by sample results of this detailed quantitative taphonomic analysis are listed in Table 2 in the supplementary data.

We have also performed a biometric analysis in order to identify patterns of variation in test size over time in two selected species of planktic foraminifera (Fig. 5): the mixed layer dweller *Pseudoguembelina hariaensis* and the intermediate dweller *Contusotruncana contusa,* one of the largest planktic foraminiferal species ever in evolutionary history. To avoid juvenile specimens, we studied the >100 μm size fraction, that was split into a representative aliquot using a microsplitter. Then, ten specimens of each

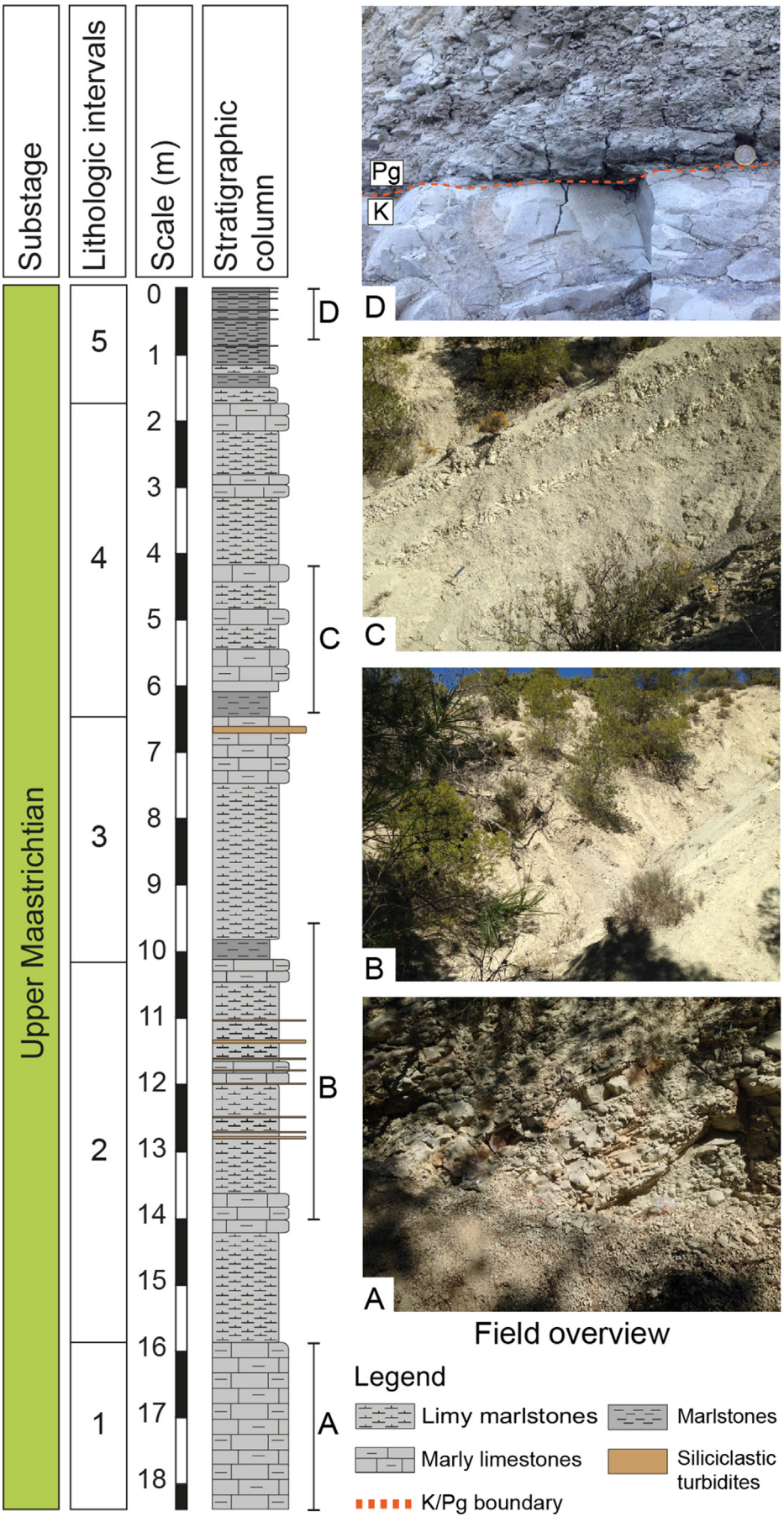

Fig. 2. Lithostratigraphic column, lithologic intervals and outcrop views of the Caravaca section. Differences between lithologies are based on $CaCO_3$ content: 75–95% for marly limestones, 65–75% for limy marlstones and 35–65% for marlstones.

Table 1
Depth related ecogroups of planktic foraminiferal genera during the late Maastrichtian.

Genera	Taxonomic group	Depth ecologies	Average relative abundance
Abathomphalus	Globotruncanids	Thermocline[1,2,3]	<0.1%
Archaeoglobigerina	Rugoglobigerinids	Intermediate[3]	0.1%
Contusotruncana	Globotruncanids	Intermediate[2,3,4,5,6]	0.1%
Globigerinelloides	Globigerinelloids	Intermediate[2,3]	8.6%
Globotruncana	Globotruncanids	Thermocline[1,2,3,6]	1.9%
Globotruncanella	Globotruncanids	Thermocline[1,2,3]	0.8%
Globotruncanita	Globotruncanids	Thermocline[1,2,3,6]	1.6%
Gublerina	Heterohelicids	Thermocline[1,2,7,10]	0.1%
Guembelitria	Guembelitrids	Mixed layer[3,8,9]	1.4%
Muricohedbergella	Hedbergellids	Intermediate[1,3,6]	6.1%
Heterohelix	Heterohelicids	Intermediate[1,2,3,4]	66.2%
Laeviheterohelix	Heterohelicids	Thermocline[1,2]	1.0%
Planoglobulina	Heterohelicids	Intermediate[1,2,3]	0.2%
Pseudoguembelina	Heterohelicids	Mixed layer[2,3,4,8]	6.8%
Pseudotextularia	Heterohelicids	Intermediate[1,2,3,4,6]	0.8%
Racemiguembelina	Heterohelicids	Intermediate[1,3,5,6]	0.4%
Rugoglobigerina	Rugoglobigerinids	Mixed layer[2,3,6,7,8]	3.5%
Plummerita	Rugoglobigerinids	Mixed layer[11]	0.1%
Schackoina	Schackoinids	Mixed layer[3]	0.3%

References: [1]D'Hondt and Arthur (1995); [2]Abramovich et al. (2003); [3]Petrizzo et al. (2020); [4]Abramovich et al. (2010); [5]Isaza-Londoño et al. (2006); [6]Falzoni et al. (2016); [7]Falzoni et al. (2014); [8]Ashckenazi-Polivoda et al. (2014); [9]D'Hondt and Zachos (1993); [10]Georgescu et al. (2008); [11]Abramovich et al. (2011).

species were randomly picked and mounted on standard 60-square micropaleontological slides. In case the aliquot did not contain ten specimens of a species, the splitting was repeated until the whole sample had been completely examined. For biometric analysis, we measured the test height and width of *P. hariaensis*, and height and length of *C. contusa* (see Fig. 5) using an Olympus UC30 digital camera connected to a Zeiss Discovery V.20 stereomicroscope, and the *Stream Image Analysis Software*. In the case of *P. hariaensis*, we differentiate two morphotypes, on the basis of the final serial arrangement of chambers: biserial, with elongated final chambers with subparallel pairs of the last few chambers (Figs. 4A and 5A), or multiserial with one or two sets of small subglobular chamberlets (Figs. 3H and 5B). Both morphotypes have previously been recognized within the inter-specific variability of *P. hariaensis* (e.g., Pl. 3, Figs. 9 and 11 of Coccioni and Premoli Silva, 2015). Biometric data and morphotype relative abundance of 507 specimens are given in Table 3 in the supplementary data.

Biometrically measured planktic foraminiferal specimens were also mounted on in a micropaleontological slide to provide a permanent record. Representative specimens of some relevant species were selected for scanning electron microscopy (SEM) analysis, and photographed using a JEOL JSM 6400 SEM at the Microscopy Service of the Universidad de Zaragoza. In order to ensure the replicability of this research, the micropaleontological material figured in this study is appropriately labelled with MPZ abbreviations (Museo Paleontológico de la Universidad de Zaragoza) and housed in the Natural Science Museum of the University of Zaragoza (Canudo, 2018).

3.2. Geochemical methods

The inorganic and organic carbonate content was measured using duplicate powdered subsamples from 87 samples that were weighed into ceramic boats, one of which was roasted in air at 420 °C for 12 h to remove organic carbon. The total carbon content of each subsample was determined using a Strohlein Coulomat 702 in the Department of Earth Sciences, University of Oxford. The difference between the amount of carbon determined in unroasted and pre-roasted samples provided an estimate of Total Organic Carbon (TOC). Reproducibility of %C using this method is typically better than 0.1%. Assuming that all the inorganic carbon is present as $CaCO_3$ allows the $CaCO_3$% to be calculated by multiplying the inorganic carbon value (from the pre-roasted sample) by 8.333 (recurring).

Stable carbon and oxygen isotopes ($\delta^{13}C$, $\delta^{18}O$) were measured using powdered bulk-rock from the same set of 87 samples. Samples were analyzed in the Department of Earth Sciences, University of Oxford using either a GasBench or a Kiel device attached to a ThermoFisher Delta V Advantage gas source isotope ratio mass spectrometer. Data are reported using the standard delta notation in per mil (‰) deviation on the VPDB scale. International and in-house standards were used to ensure the comparability between instruments and the precision and accuracy of the data. Repeated analyses of in-house standards suggest a reproducibility ($\pm 1\sigma$) of <0.1 for both $\delta^{13}C$ and $\delta^{18}O$.

4. Results

4.1. Planktic foraminiferal turnover

At Caravaca, planktic foraminiferal assemblages are characterized by a high diversity and a wide range of size and morphological variability of the tests. Species richness from the base to the top of the studied section remains very high with values between 63 and 69 species per sample. A total of 70 species belonging to 20 genera have been identified throughout the section (Fig. 6 and Table 1 in the supplementary data). Within the interval from 13.80 to 5.05 m below the KPB, the average species richness value is slightly lower (Fig. 7A). This is due to the disappearance of scarcer species, such as *Archaeoglobigerina cretacea*, *A. blowi*, *Globotruncanita falsocalcarata*, *Abathomphalus intermedius* and *Contusotruncana patelliformis*, that are absent in >20% of the analyzed samples. At Caravaca, we have identified the highest occurrences (HO) of only 4 species: HO of *A. cretacea* at 50 cm below the KPB, HO of *Gita. falsocalcarata* at 40 cm below the KPB, HO of *A. blowi* at 15 cm below the KPB, and HO of *Planoglobulina manuelensis* at 1 cm below the KPB. All remaining 66 planktic foraminiferal species have been identified in the uppermost sample, just 1 cm below the KPB (Table 1 in the supplementary data).

Quantitative data are shown in Table 2 of the supplementary material and plotted in Figs. 7 and 8. The P/B ratio always exceeds 95% (Fig. 7B), suggesting pelagic conditions and a relatively stable paleobathymetry throughout the Caravaca section. Given these broad and stable environmental conditions, it is no surprise that all Maastrichtian planktic foraminiferal ecogroups are well represented (e.g., heterohelicids, pseudoguembelinids, globotruncanids, rugoglobigerinids, hedbergellids, globigerinelloids and schackoinids).

Changes in the deep/surface (D/S) ratio allow us to differentiate three intervals (Fig 7C). In the lower part of the studied section (18.30–13.20 m below the KPB), the D/S ratio varies between 0.28 and 0.52, with an average of 0.39. The lowest D/S ratio values in the Caravaca section have been identified from 13.20 to 5.05 m below the KPB. Within this interval, D/S ratio values range between 0.0 and 0.45, with an average of 0.20. From 5.05 m to the KPB, D/S ratio values range between 0.29 and 0.47, with an average value of 0.39.

Planktic foraminiferal assemblages in the >63 μm size fraction are dominated by the generalist *Heterohelix*, with an average relative abundance of about 66% (Fig. 8). Other common genera are *Globigerinelloides* (8.6%), *Pseudoguembelina* (6.8%) and *Muricohedbergella* (6.1%). On average, the least abundant genera are *Rugoglobigerina* (3.5%), *Globotruncana* (1.9%), and *Globotruncanita* (1.6%). In Fig. 8, other genera whose average relative abundance is

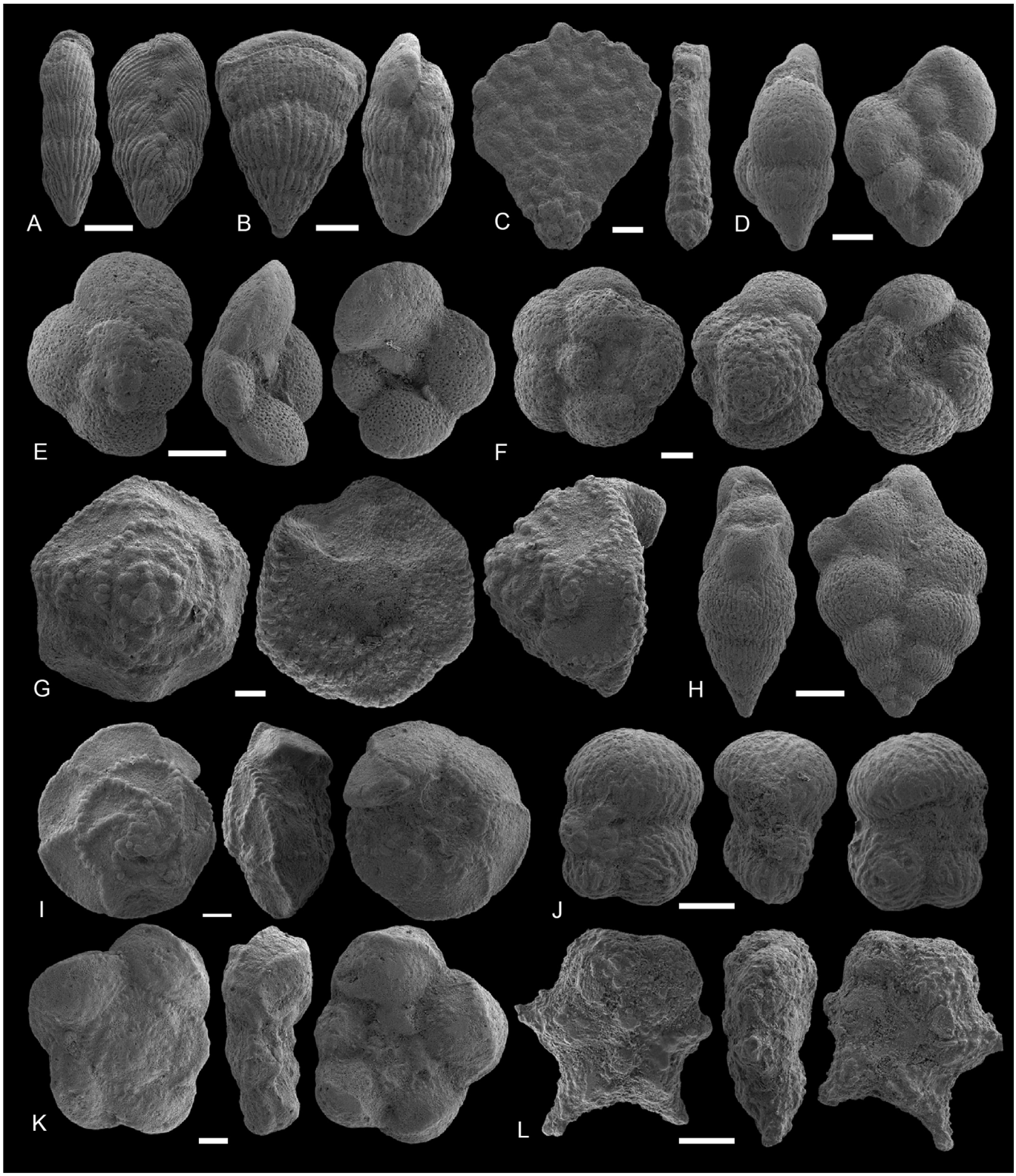

Fig. 3. Examples of moderate to good preserved tests of planktic foraminiferal species from the Caravaca section (scale bars = 100 μm): **A)** *Pseudoguembelina costulata*, sample GR-0-2 (MPZ 2019/1), **B)** *Pseudotextularia elegans*, sample GR-0-2 (MPZ 2019/2), **C)** *Planoglobulina multicamerata*, sample GR-0-2 (MPZ 2019/3), **D)** *Pseudoguembelina palpebra*, sample GR-0-2 (MPZ 2019/4), **E)** *Globotruncanella petaloidea*, sample GR-0-2 (MPZ 2019/5), **F)** *Rugoglobigerina rotundata*, sample GR-4-6 (MPZ 2019/6), **G)** *Contusotruncana contusa*, sample GR-4-6 (MPZ 2019/7), **H)** *Pseudoguembelina hariaensis*, multiserial morphotype sample GR-4-6 (MPZ 2019/8), **I)** *Globotruncanita stuarti*, sample GR-4-6 (MPZ 2019/9), **J)** *Rugoglobigerina macrocephala*, sample GR-10 (MPZ 2019/10), **K)** *Abathomphalus mayaroensis*, sample GR-110 (MPZ 2019/11), **L)** *Plummerita hantkeninoides*, sample GR-630 (MPZ 2019/12).

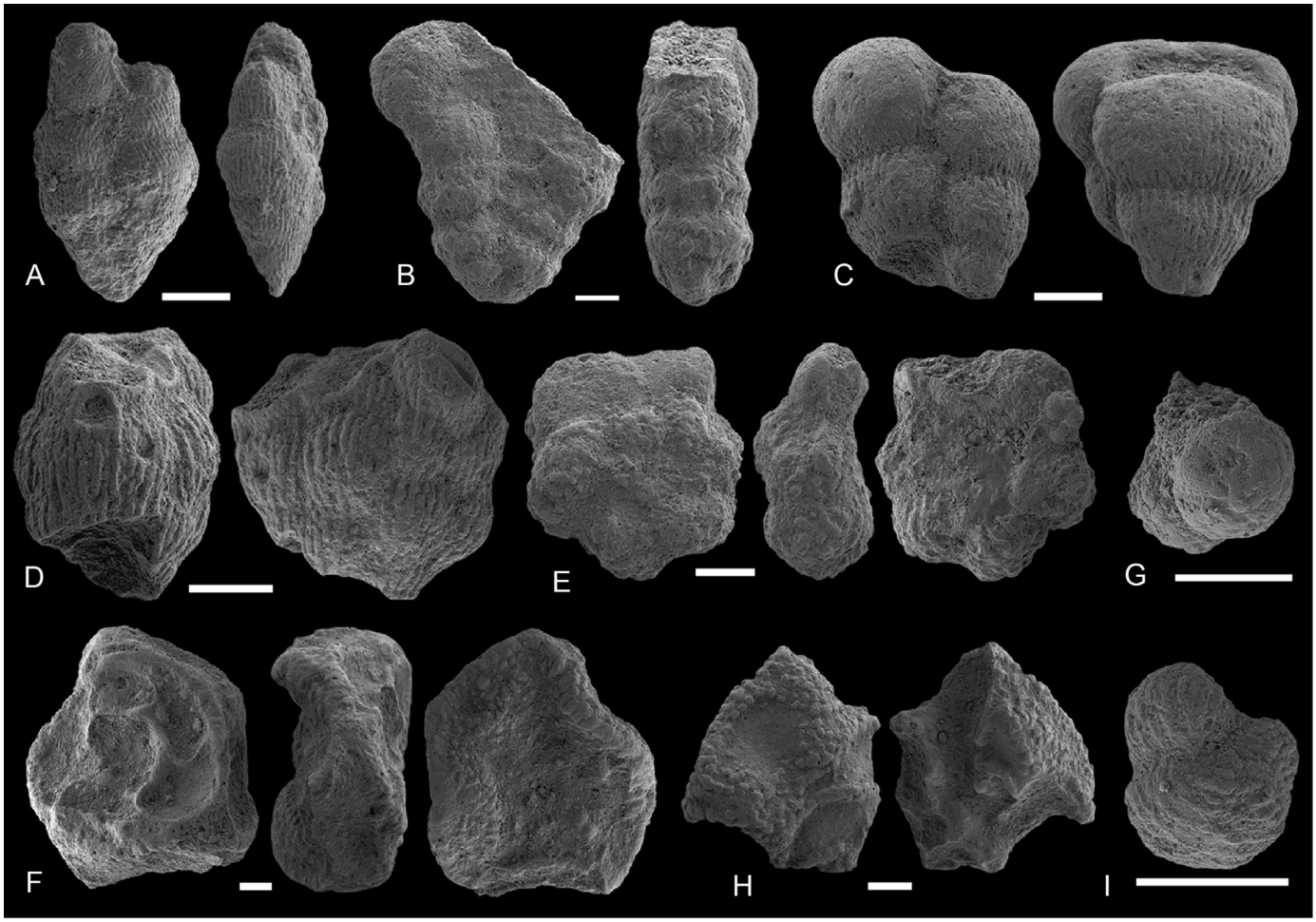

Fig. 4. Examples of poor preservation and fragmentation in planktic foraminiferal tests from the Caravaca section (scale bars = 100 μm): **A)** *Pseudoguembelina hariaensis,* biserial morphotype sample GR-1830 (MPZ 2019/13), **B)** *Gublerina cuvillieri,* sample GR-1380 (MPZ 2019/14), **C)** *Pseudotextularia nutalli,* sample GR-1020 (MPZ 2019/15), **D)** *Planoglobulina acervulinoides,* sample GR-655 (MPZ 2019/16), **E)** *Rugoglobigerina hexacamerata,* sample GR-1380 (MPZ 2019/17), **F)** *Contusotruncana contusa,* sample GR-1080 (MPZ 2019/18), **G)** fragment indet., sample GR-1290 (MPZ 2019/19), **H)** globotruncanid fragment sample GR-1290 (MPZ 2019/20), **I)** fragment indet., sample GR-655 (MPZ 2019/21).

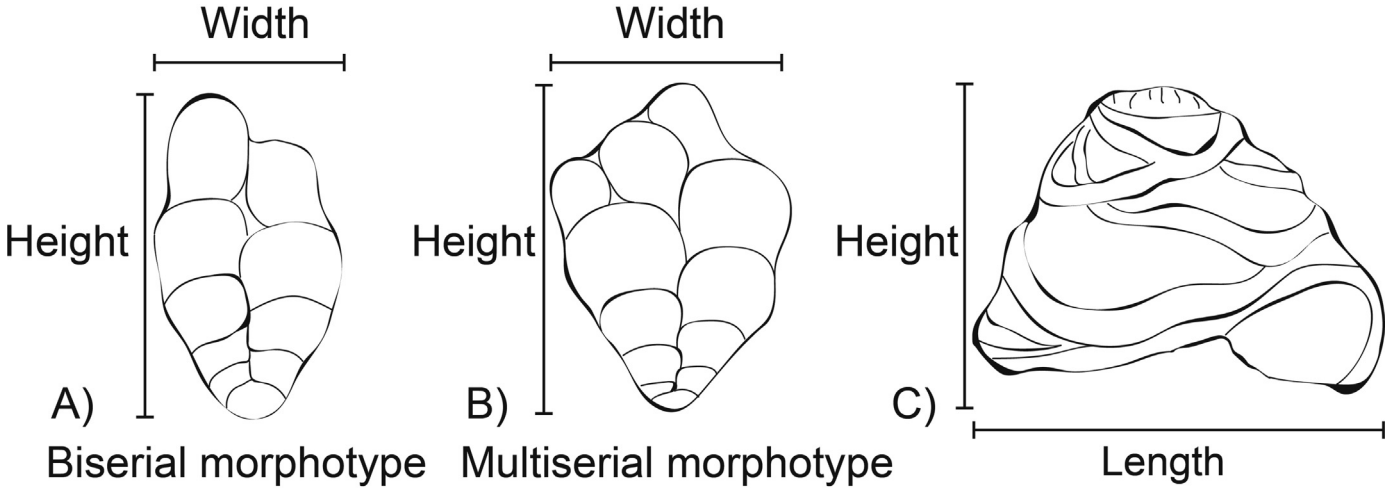

Fig. 5. Biometric variables measured on the tests of selected species and morphotypes. A) Biserial morphotype of *Pseudoguembelina hariaensis*; B) Multiserial morphotype of *P. hariaensis*; C) *Contusotruncana contusa*.

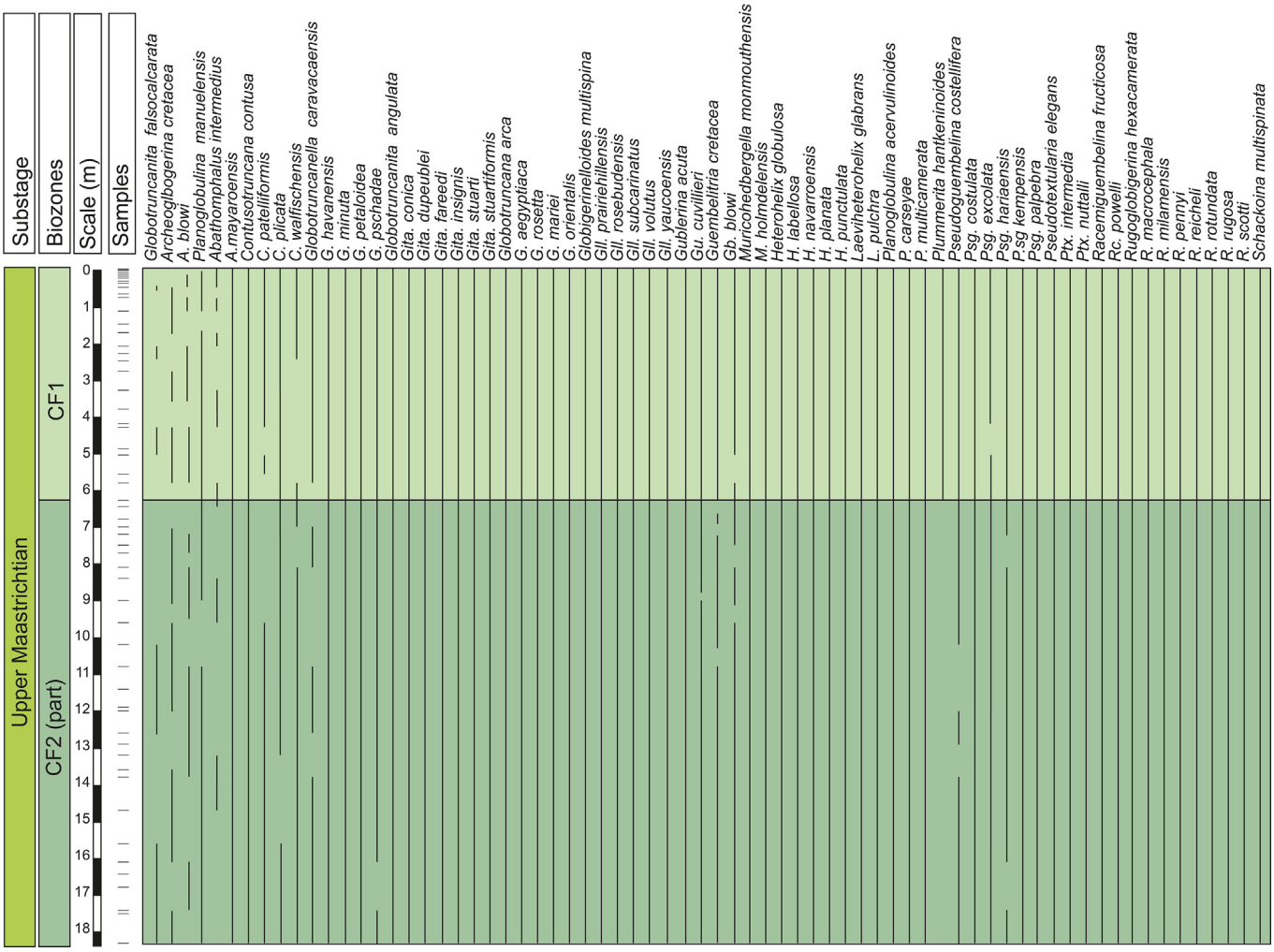

Fig. 6. Stratigraphic distribution of the late Maastrichtian planktic foraminiferal species.

<1% are grouped together. This group is composed of the following genera: *Abathomphalus, Archaeoglobigerina, Contusotruncana, Globotruncanella, Gublerina, Planoglobulina, Pseudotextularia, Racemiguembelina, Plummerita* and *Schackoina*.

4.1.1. Planktic foraminiferal size and morphological variation

We evaluated changes in test size of two planktic foraminiferal species: *Contusotruncana contusa* (intermediate dweller) and *Pseudoguembelina hariaensis* (mixed layer dweller). Biometric data are provided in Supplementary Table 3 and plotted in Fig. 9. The variation in test size of *C. contusa* is remarkable, especially between 13.8 and 5.05 m below the KPB (Fig. 9A). In this interval, the size reduction is close to 35% and occurs almost equally on both height and length of the test. Conversely, *P. hariaensis* was not affected by dwarfing, since its size progressively increases across the section (Fig. 9B). However, the relative abundance of the two morphotypes of *P. hariaensis* also varies remarkably between 13.2 and 5.05 m below the KPB (Fig. 9C). The biserial morphotype, with elongated final chambers, became more abundant within this depth interval, with a mean relative abundance of about 75%. Multiserial morphotypes, with small chamberlets, tend to dominate below and above this depth interval.

4.1.2. Planktic foraminiferal fragmentation index (FI)

We have recognized FI values higher than 40% in ten samples within two intervals: from 15.60 to 10.80 m and from 7.50 to 6.30 m below the KPB (Table 2 in the supplementary data and Fig. 10A). Large oscillations in the FI are identified within both intervals, suggesting relatively rapid changes in carbonate dissolution intensity. Nonetheless, most of the studied section is below a moderate/strong dissolution limit of FI < 40% especially in the uppermost 6 m of the Maastrichtian. Linear regressions between FI and $CaCO_3$ content (Fig. 10B) and between FI and P/B ratios (Fig. 10C) show null and poor correlation coefficients.

4.2. Geochemistry

Total organic carbon (TOC) is less than 0.2%, or below detection limits in some samples, so, these data are not discussed further. % $CaCO_3$ varies from 55.4% to 82.0%, with a mean value of 72.7% ($\pm1\sigma$ = 5%, n = 87). Stratigraphically there is little variability (Table 4 in the supplementary data), with small scale-fluctuations representing lithological differences between marlstones, marly limestones and limy marlstones.

Carbon-isotope ($\delta^{13}C$) values vary between −0.60 and + 2.12‰ with a mean of +1.44‰ ($\pm1\sigma$ = 0.51‰, n = 87; Table 4 in the supplementary data). Oxygen-isotope ($\delta^{18}O$) values vary between −3.17 and −1.80‰, with a mean of −2.21‰ ($\pm1\sigma$ = 0.26‰, n = 87). The isotopic data exhibit broad stratigraphic trends, with higher resolution variability superimposed upon these (Fig. 11). At a broad scale across the entire record, both carbon and oxygen isotopes exhibit a broad decrease to minimum values between 13.80

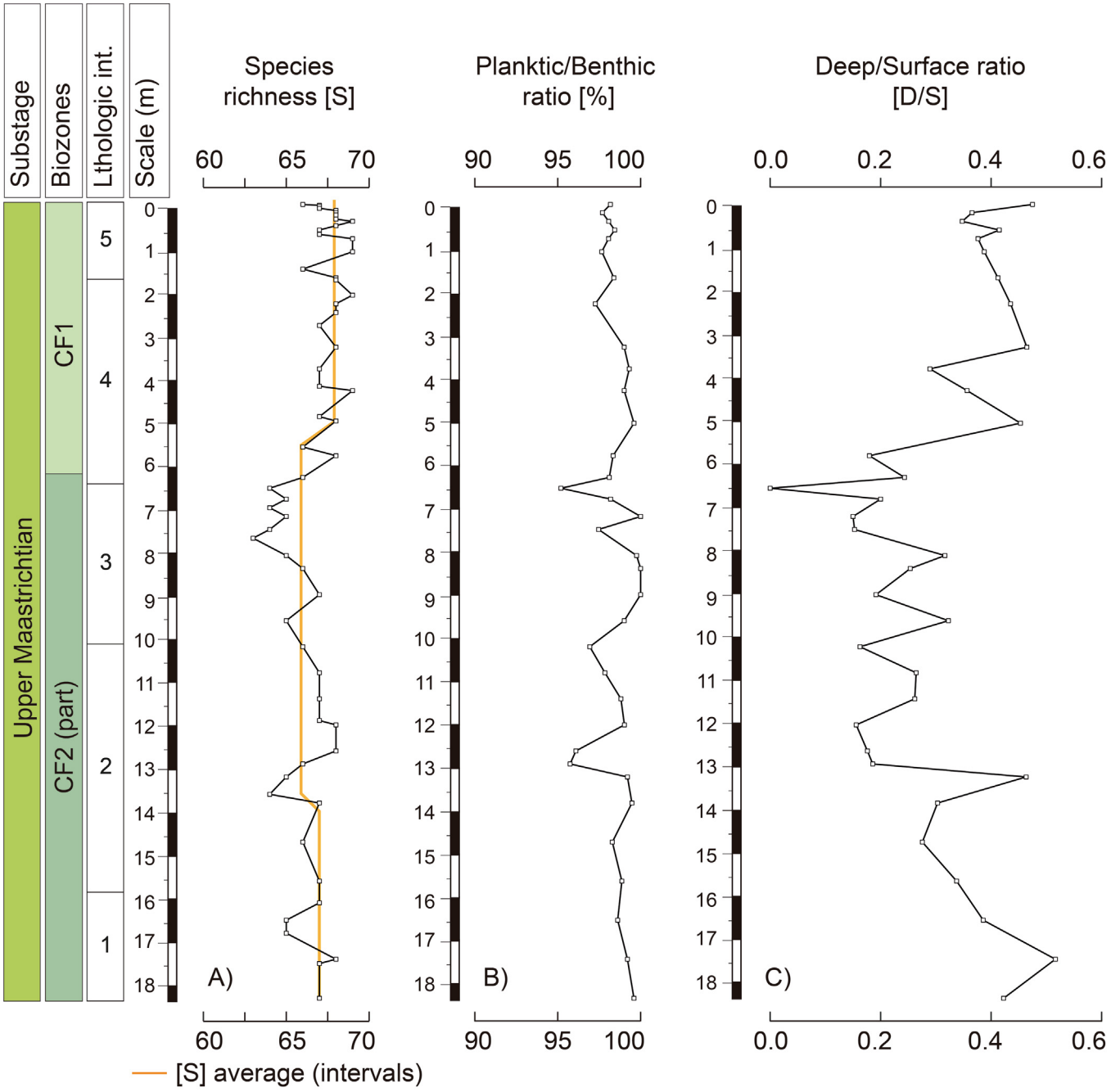

Fig. 7. Shifts in species richness (S), planktic/benthic (P/B) ratio and deep/surface (D/S) ratio.

and 5.05 m below the boundary before increasing prior to the KPB. In detail, there are notable negative excursions from the broad pattern in both $\delta^{18}O$ and $\delta^{13}C$, occurring at 10.80 m, 6.55 m and 6.30 m below the KPB.

5. Biostratigraphy and age model

Only the last two biozones of Li and Keller (1998b) alphanumerical scale, Zones CF1 (*Plummerita hantkeninoides*) and CF2 (*Pseudoguembelina palpebra*), have been identified at Caravaca (Fig. 6). The lowest occurrence (LO) of *Plummerita hantkeninoides*, the base of Zone CF1, is located 6.3 m below the KPB. In this biohorizon, we found the first indubitable specimens of *P. hantkeninoides* with well-developed tubulospines in the last whorl (Fig. 3L), although proto-*P. hantkeninoides* transitional forms with rugosities and some elongated chambers (but not true tubulospines) are found from 6.8 m below the KPB. The HO of *Gansserina gansseri*, the base of Zone CF2, has not been recognized since it occurs >18.3 m below the KPB, within strata that are no longer exposed and were, thus, inaccessible to us. Through the whole stratigraphic section, there is no evidence of erosive surfaces or abrupt changes in lithology, so we assume that the sedimentation rate was rather stable across the studied interval.

We have used the Husson et al. (2014) calibration for the Cretaceous part of the C29r magnetochron, which is based on the astrochronological age model from the Contessa Highway and

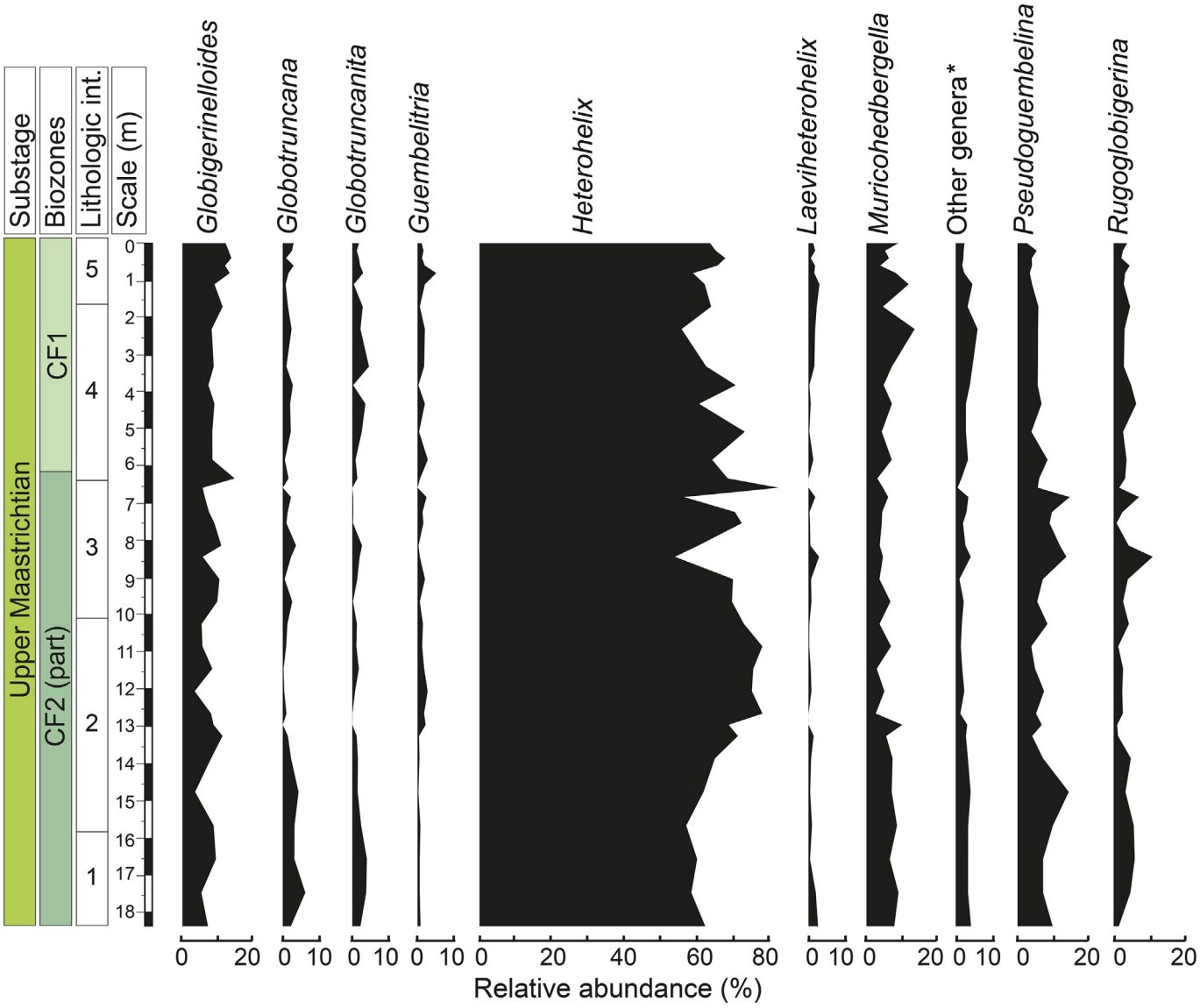

Fig. 8. Quantitative stratigraphic distribution of planktic foraminiferal genera. Other genera includes: *Abathomphalus, Archaeoglobigerina, Contusotruncana, Globotruncanella, Gublerina, Planoglobulina, Pseudotextularia, Racemiguembelina, Plummerita* and *Schackoina*.

Bottaccione sections near Gubbio, Italy. This age model provides a duration for the Cretaceous part of C29r of ~365 kyr, very similar to that given by GTS 2012 (~358 kyr, Gradstein et al., 2012). Following Renne et al. (2013), the KPB is dated at 66.04 Ma in both time scales. Husson et al. (2014) provided calibrated ages for micropaleontological data, such as the LO of *P. hantkeninoides* at 140 kyr before the KPB. The KPB and the LO of *P. hantkeninoides* have been used as tie points to estimate the linear sedimentation rate of the entire Caravaca section, resulting in an average of 4.5 cm/kyr.

At Bottaccione (Gubbio), the LO of *P. hantkeninoides* and HO of *G. gansseri* are, respectively, 1.4 and 4.7 m below the KPB (Husson et al., 2014; Coccioni and Premoli Silva, 2015). Assuming a constant sedimentation rate of 4.5 cm/kyr for Caravaca and correlating with planktic foraminiferal data from Gubbio, the HO of *G. gansseri* should be located 21.15 m below the KPB of Caravaca, so the studied section spans approximately the uppermost 80% of Zone CF2. In this age framework, the materials studied and discussed here span the last ~400 kyr of the Maastrichtian.

6. Global correlation of the isotope record and Latest Maastrichtian Warming Event

6.1. Veracity of the isotope records

Bulk stable-isotope records from pelagic marls, chalks and limestones have been used extensively for chemostratigraphic correlation and for reconstructing trends in Cretaceous climate (e.g., Scholle and Arthur, 1980; Jenkyns et al., 1994; Clarke and Jenkyns, 1999; Jarvis et al., 2006). However, before interpreting such data as a record of primary signals from Cretaceous seawater, diagenetic effects must be discounted. The $\delta^{13}C$ and $\delta^{18}O$ data from Caravaca presented here have values that are consistent with carbonate formation from Late Cretaceous seawater (Table 4 in the supplementary data) and are comparable to previous studies from the KPB interval itself at Caravaca (Kaiho and Lamolda, 1999; Sosa-Montes de Oca et al., 2016). A cross plot (Fig. 12C) shows that a positive correlation exists between $\delta^{13}C$ and $\delta^{18}O$. Although this

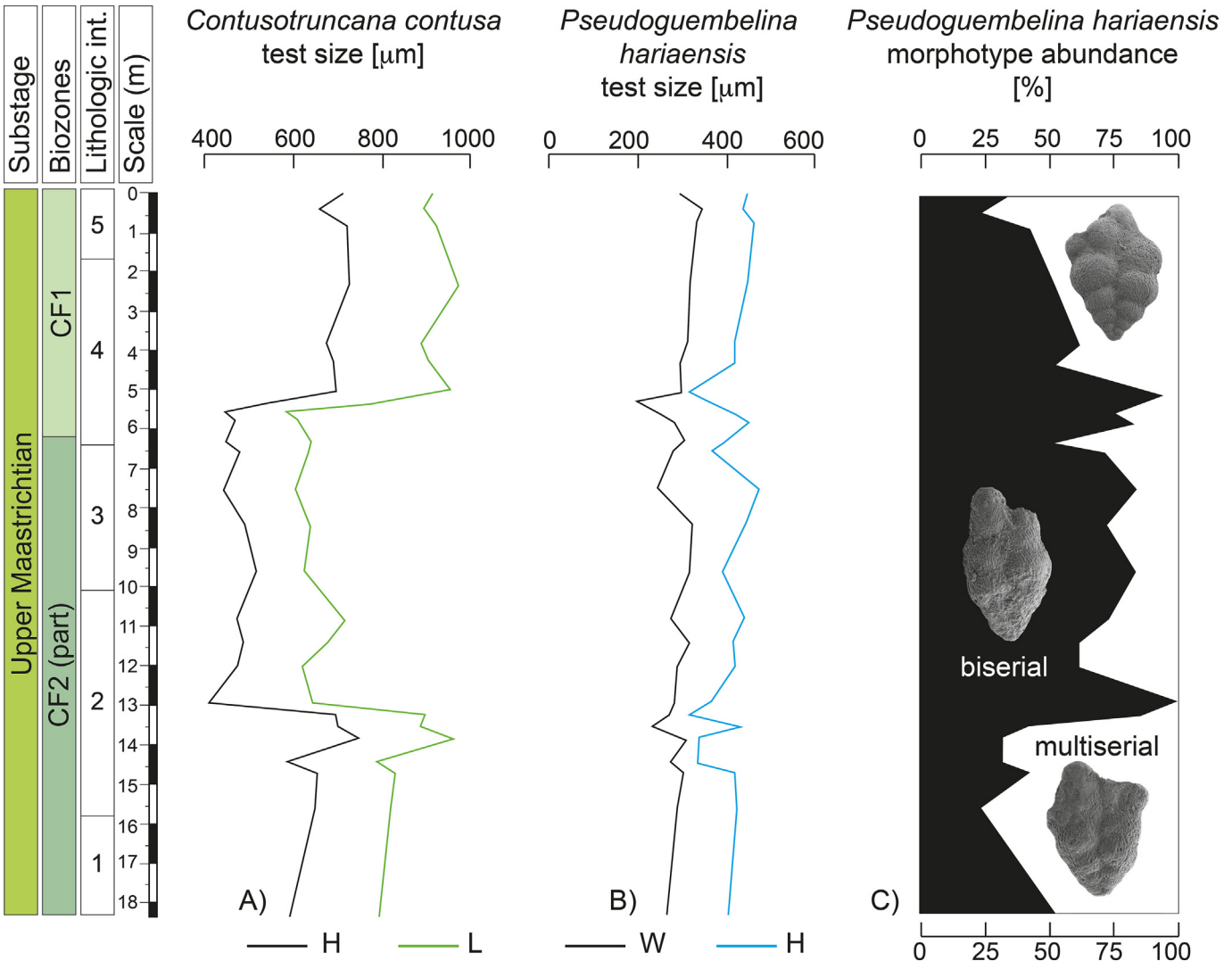

Fig. 9. Changes in the test size of *C. contusa* (A) and *P. hariaensis* (B), and in the relative abundance of *P. hariaensis* biserial morphotype (C).

relationship could be an indicator of a minor contribution of diagenetic calcite (with isotopically low $\delta^{13}C$ and $\delta^{18}O$ values).

Three samples, in particular, appear to have slightly lower $\delta^{13}C$ and $\delta^{18}O$ values than the remainder of the dataset and could, therefore, be outliers as a consequence of either unknown analytical issues, a more significant contribution of diagenetic calcite or short-term warming events associated with isotopically lighter DIC. When plotted stratigraphically, these three samples with relatively low $\delta^{13}C$ and $\delta^{18}O$ values (highlighted in Fig. 13) are offset from the remainder of the dataset. However, we note that they occur within intervals of relatively low background values and that 'extreme' values are within the broad range of possible seawater values recorded by pelagic sediments. We cannot exclude the possibility that these samples are outliers (as a consequence of diagenesis or analysis) but we have no analytical or geological justification for excluding them entirely from the dataset at this point.

Overall, the small range of oxygen-isotope values, their absolute value, and the moderate to good preservation of the planktic foraminifer are not consistent with extensive burial diagenesis nor the influence of meteoric waters. Furthermore, there is no relationship between $\%CaCO_3$ and the stable-isotope data (Figs. 12A-B), suggesting that lithology exerts little control on the measured isotope values. There are statistically significant negative relationships between the fragmentation index and both $\delta^{13}C$ and $\delta^{18}O$ (Figs. 12D-E), but with very weak correlation coefficients. These relationships could suggest that differential degrees of dissolution of some carbonate components (most likely planktic foraminifera) may be contributing to the covariance of $\delta^{13}C$ and $\delta^{18}O$, but the weak regression coefficients suggest that, if true, this cannot be a major effect. We cannot constrain absolute paleotemperatures from the $\delta^{18}O$ data with confidence due to varying sources of carbonate within the sediment, but given the dominance of calcareous plankton observed by us, the isotopic trends presented here likely reflect the average isotopic signature of the planktic dwellers of the upper part of the water column. In light of the considerations discussed here, we suggest that the stable-isotope data from Caravaca most likely reflect primary trends in Maastrichtian seawater chemistry and temperature.

6.2. Identifying the LMWE at Caravaca

The Maastrichtian was a relatively cool period in the Late Cretaceous, following the long-term cooling trend in the Campanian (e.g. Huber et al., 1995, 2018; Linnert et al., 2014; O'Brien et al.,

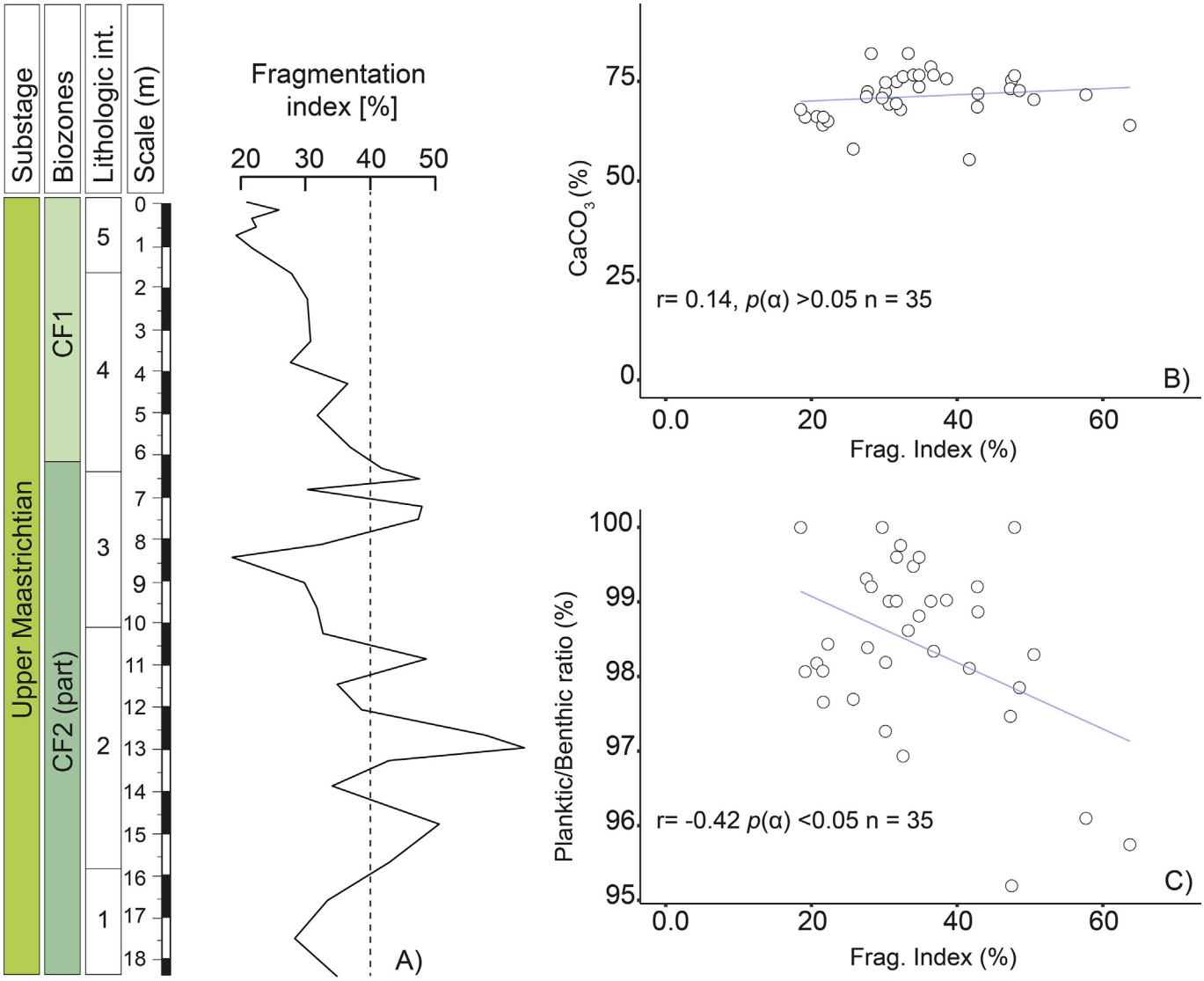

Fig. 10. Changes in fragmentation index (FI) (A), cross-plots between $CaCO_3$% and FI (B), and cross-plots between $CaCO_3$% and P/B ratio (C).

2017; O'Connor et al., 2019). During the Maastrichtian itself, a number of relatively minor fluctuations in climate have been recorded in widespread localities, most notably the brief warming episode of LMWE, ~300-150 kyr before the KPB (Barrera and Savin, 1999; MacLeod et al., 2005; Huber et al., 2018). The LMWE has previously been identified from globally distributed sites and sections, typically by $\delta^{18}O$ and has been commonly related to the onset of the main eruptive phase of the Deccan Traps (e.g. Dessert et al., 2001; Keller et al., 2008; Tobin et al., 2012; Husson et al., 2014; Barnet et al., 2018, 2019; Schoene et al., 2019; Hull et al., 2020).

In Fig. 13, we compare the isotopic record from the Caravaca section with isotopic datasets from the Southern Ocean ODP Site 690 (Stott and Kennet, 1990), the South Atlantic DSDP Site 525A (Li and Keller, 1998a), the central Pacific Site ODP1209 (Westerhold et al., 2011), the South Atlantic ODP Site 1262 (Barnet et al., 2018), the Newfoundland Margin Site U1403 (Batenburg et al., 2018), the Gubbio section, Italy (Voigt et al., 2012) and Zumaia section, northern Spain (Batenburg et al., 2012). Age models for ODP Site 1209 (Westerhold et al., 2011), ODP Site 1262 (Barnet et al., 2018), IODP U1403 (Batenburg et al., 2018) and Zumaia (Batenburg et al., 2012) are based on cyclostratigraphy. Age models for the other localities are based on interpolated ages using those estimated for the base of C29r, KPB and LO of *P. hantkeninoides* by Husson et al. (2014). For a better comparison of the different datasets, we applied the KPB age of 66.04 Ma estimated by Renne et al. (2013) to all localities.

At Caravaca and the ODP/IODP Sites (Fig. 13), the $\delta^{18}O$ records all show an interval characterized by relatively low $\delta^{18}O$ values between 66.35 and 66.14 Ma (i.e., between 310 and 100 kyr before the KPB), which was preceded and followed by higher $\delta^{18}O$ isotope values. This interval has been previously recognized as the LMWE at some of these sites (e.g., Abramovich and Keller, 2003; Thibault and Gardin, 2010; Woelders et al., 2017; Barnet et al., 2018, 2019). As there are local differences between the different datasets, we propose, that the generally warm episode identified at the Caravaca section is the local isotopic record of the LMWE.

Previous work by Voigt et al. (2012) has postulated the existence of a consistent pattern of $\delta^{13}C$ change immediately prior to the KPB at several sites, with relatively positive values around the C29r/C30n boundary (KPg-2 event of Voigt et al., 2012), followed by a negative excursion (KPg-3 event) before a final positive event within which the KPB itself occurs (not named by Voigt et al., 2012).

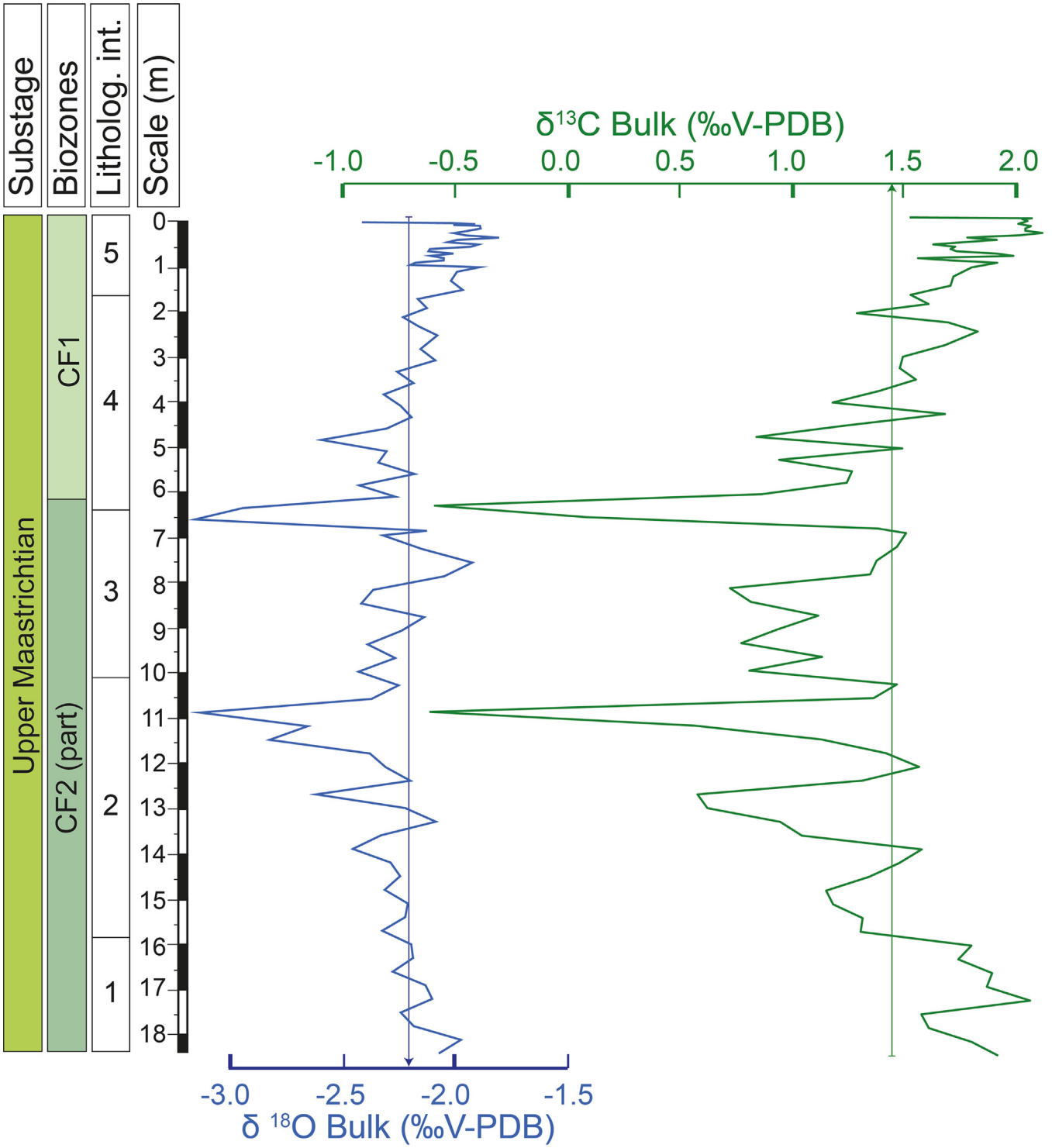

Fig. 11. Changes in $\delta^{13}C$ and $\delta^{18}O$ across the Caravaca section, the arrows mark the mean value for each isotope.

At Caravaca, it is possible that the positive values at the base of the section correspond to part of KPg-2, followed by lower $\delta^{13}C$ values associated with the LMWE (KPg-3) and then a return to more positive values at the KPB. At Site 525, the highest occurrence of *G. gansseri* is associated with the KPg-2 event (Voigt et al., 2012), which, given that this same foraminiferal event must occur below the base of the section at Caravaca, implies that Caravaca contains only a partial record of the KPg-2 event. Fig. 13 illustrates that precise correlation of the carbon isotope events prior to the KPB is problematic, as there is not perfect consistency between records of these (rather small magnitude) events when viewed at such high resolution, possibly as a consequence of age model limitations and uncertainties, sampling resolution, carbonate type, and/or site-specific oceanographic and diagenetic conditions. It is only during the last ~100 kyr of the Maastrichtian that there is a clearer consistency in $\delta^{13}C$ trends with many records, including Caravaca,

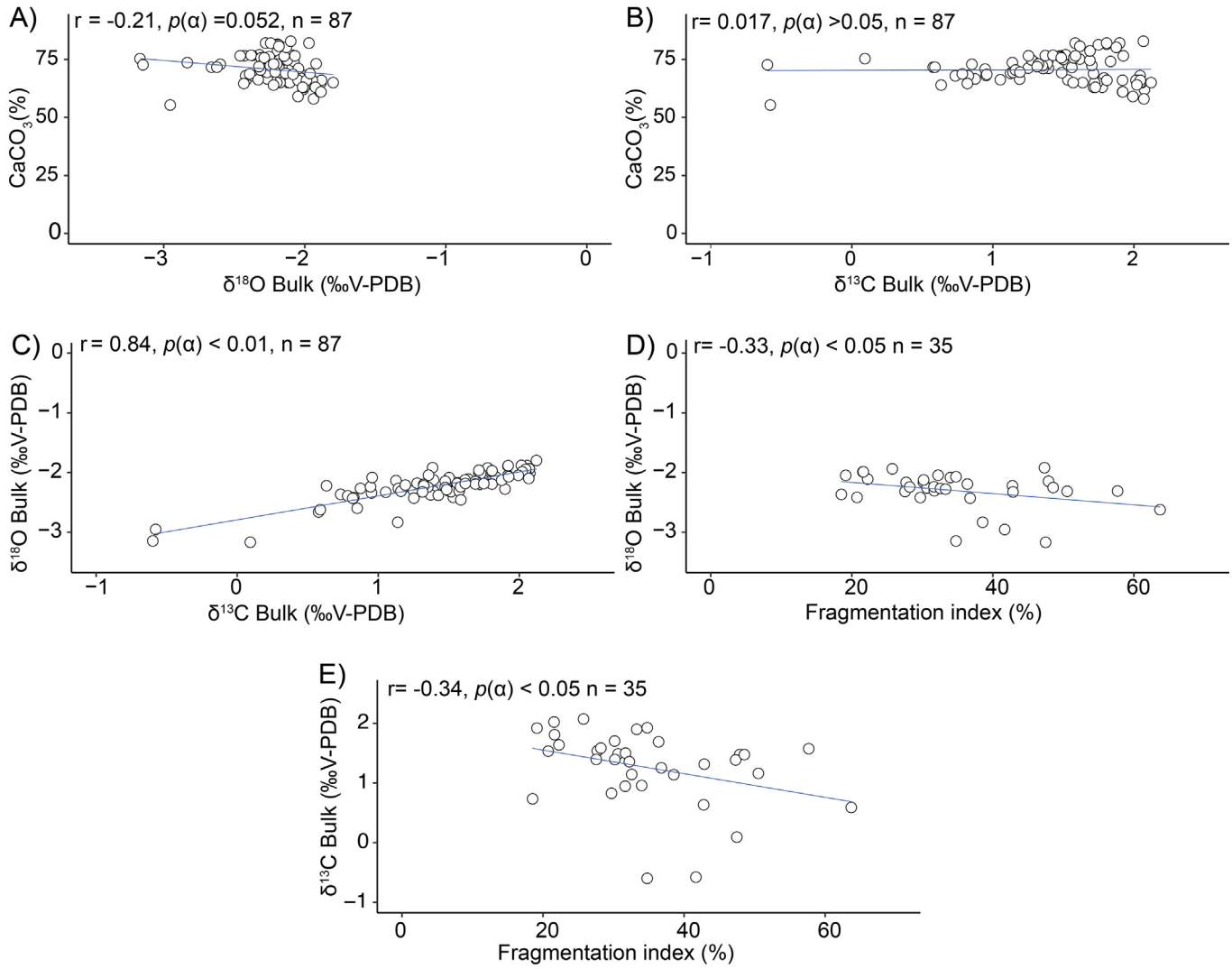

Fig. 12. Cross-plots between $CaCO_3$% and $\delta^{18}O$ (A), $CaCO_3$% and $\delta^{13}C$ (B), $\delta^{18}O$ and $\delta^{13}C$ (C), $\delta^{13}C$ and FI (D), and $\delta^{18}O$ and FI (E).

exhibiting a small increase in $\delta^{13}C$ towards the KPB (Fig. 13). Intriguingly, at both Zumaia and Caravaca, there are some remarkable negative excursions in $\delta^{13}C$ bulk values (Fig. 13; Batenburg et al., 2012) which are very close in age at both localities. However, uncertainties in the precise age assignments of these isotope events, and questions over their veracity as primary seawater signals (as discussed in Section 6.1 above), prevents us from concluding that they are simultaneous events and requires further work in order to determine if these events have any significance.

7. Planktic foraminiferal response to LMWE

In this study, the planktic foraminiferal proxies presented provide evidence for environmental and climatic disturbances at Caravaca during the LMWE between 66.35 and 66.14 Ma, i.e. between 310 and 100 kyr before the KPB (Figs. 14 and 15). The evidence for changes in the upper water column environment are as follows:

First, specific richness (S) slightly decreases during the LMWE, due to temporary disappearances (Lazarus effect) of some scarce species. Lazarus-taxa, such as *Gita. falsocalcarata, C. patelliformis* or *A. intermedius,* reappeared when the waters returned (marked by an increase in $\delta^{18}O$) to cooler conditions similar to the pre-LMWE phase.

Second, the Deep/Surface (D/S) ratio is 2–4 times higher in the pre- and post-LMWE intervals, compared to the LMWE itself. Similar ecological replacement has been observed in the late Maastrichtian at South Atlantic DSDP Site 525A, where the climate warming de-stratified the upper water column causing the removal of deep habitat niches (Abramovich and Keller, 2003).

Third, changes in the relative abundances of some genera, such as the increase in the low-oxygen tolerant genus *Heterohelix* (Pardo and Keller, 2008), indicate lower oxygen levels in the upper part of the water column during the LMWE. The relative abundance of *Heterohelix* increases in the intervals from 13.80 to 9.00 m and 7.50 to 5.05 m below the KPB, reaching maximum values between 78 and 82% in the samples at 12.60, 10.80, and 6.55 m below the KPB. Based on the $\delta^{18}O$ record from Caravaca, the *Heterohelix* maxima coincide with the warmer events during the LMWE, probably driven by a decrease of seawater oxygen solubility in this area of the western Tethys. Seawater oxygen solubility is a limiting factor that decreases with increasing temperature since surface-water oxygen concentrations depend on the mixed-layer temperature (Helm et al., 2011). Between the two *Heterohelix* maxima, a discrete and

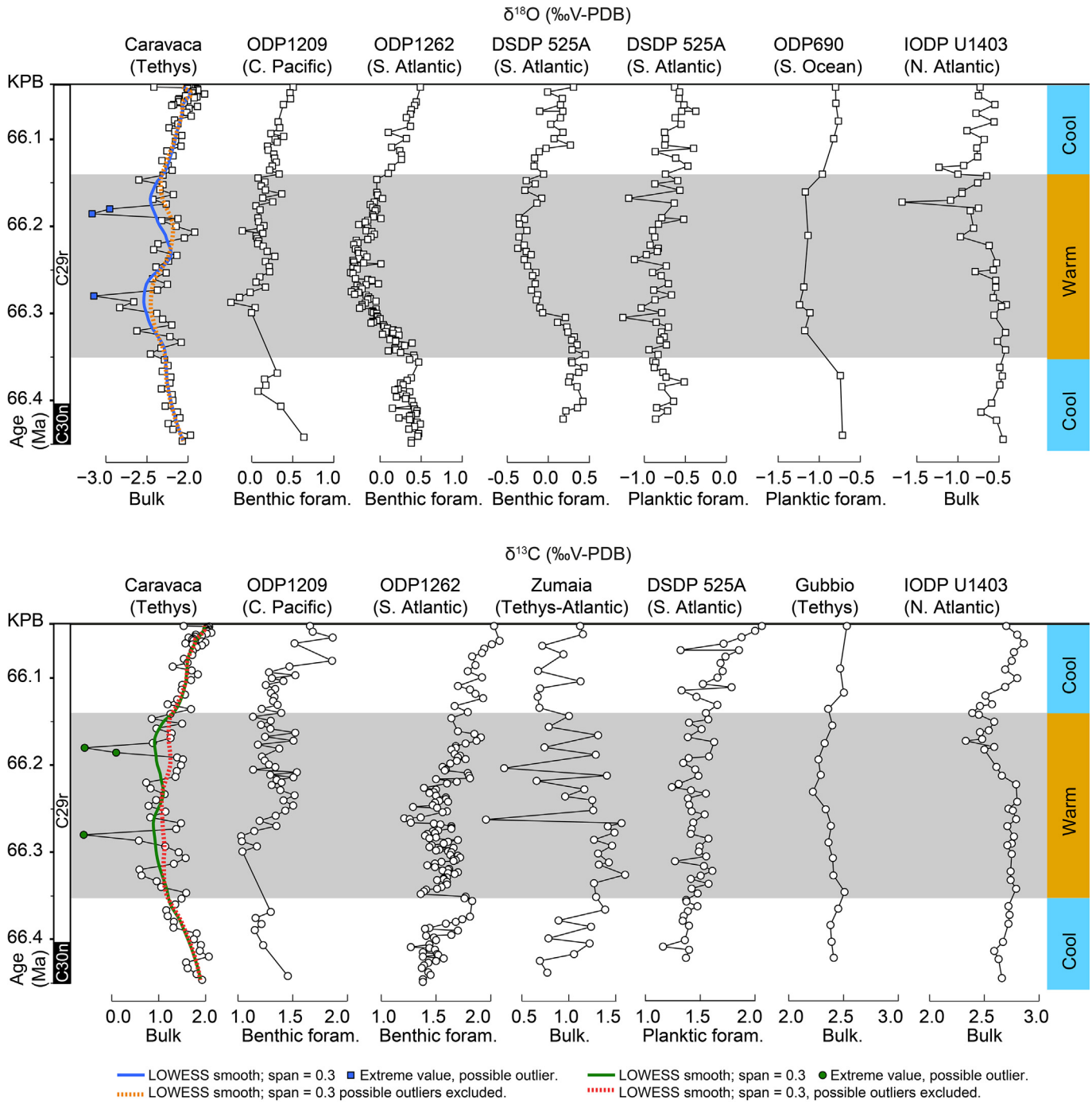

Fig. 13. Correlation of the $\delta^{13}C$ and $\delta^{18}O$ record from several upper Maastrichtian localities worldwide: Caravaca, this study; Southern Ocean ODP Site 690 (Stott and Kennet, 1990); South Atlantic DSDP Site 525A (Li and Keller, 1998a); central Pacific Site ODP1209 (Westerhold et al., 2011); South Atlantic ODP Site 1262 (Barnet et al., 2018); North Atlantic Newfoundland Margin Site U1403 (Batenburg et al., 2018); Zumaia (Batenburg et al., 2012); Gubbio (Voigt et al., 2012). Time-scale (Ma) is based on Husson et al. (2014).

temporary increase in *Pseudoguembelina*, globotruncanids and rugoglobigerinids is observed, which could reflect short intervals of better environmental conditions. Significantly, no increase in the disaster opportunist *Guembelitria* is identified across this interval (Fig. 8). *Guembelitria* blooms are often considered indicators of widespread high-stress conditions during the late Maastrichtian (Abramovich and Keller, 2002; Pardo and Keller, 2008; Punekar et al., 2014).

Fourth, an increase in the abundance of the biserial morphotype of *P. hariaensis* with elongated terminal chambers during the LMWE could be related to a lower seawater oxygen solubility. Throughout the evolutionary history of the planktic foraminifera, the elongation of the terminal chambers is commonly associated with a reduced oxygenation of the water column (BouDagher-Fadel et al., 1997; Premoli Silva et al., 1999; Coccioni et al., 2006; Luciani et al., 2007). Luciani et al. (2007) considered the chamber elongation in planktic foraminifera as a recurring morphological character that constitutes an adaptation to facilitate oxygen uptake in a poorly oxygenated environment by increasing the surface/volume ratio of chambers.

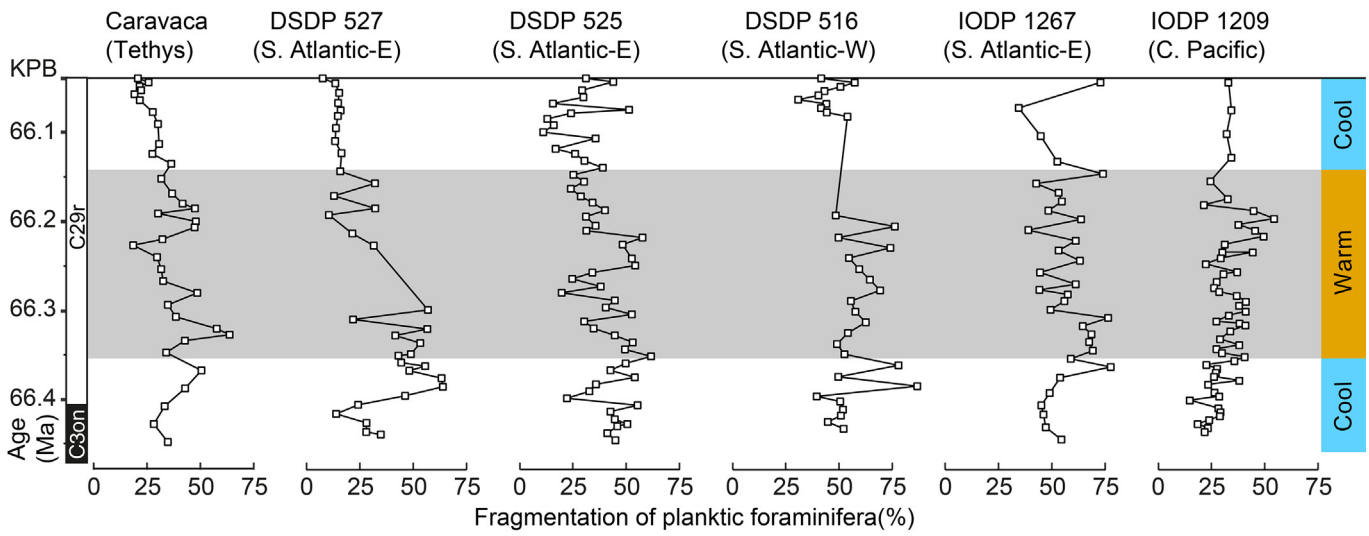

Fig. 14. Correlation of the planktic foraminiferal fragmentation record from several upper Maastrichtian localities worldwide: Caravaca, this study; South Atlantic DSDP 527, 525 and 516 (Kucera et al., 1997); South Atlantic IODP 1267 and Central Pacific IODP 1209 (Henehan et al., 2016). Time-scale (Ma) is based on Husson et al. (2014).

Fifth, the LO of *P. hantkeninoides* occurs within the upper part of the LMWE interval in Caravaca and many other localities (Husson et al., 2014). This species exhibits elongated chambers and well-developed tubulospines in the last whorl. We speculate that this morphology was an adaptation to inhabit deep waters with lower dissolved oxygen levels. Later, when global temperature decreased, and water-column stratification was reestablished, this species could migrate into fully oxygenated near-surface waters. A similar hypothesis was proposed by Coccioni et al. (2006), for planktic foraminiferal species with well-developed tubulospines such as the Eocene hantkeninids. However, further studies, from more localities, are necessary to establish the validity of a possible relationship between decreased dissolved oxygen during the LMWE and development of elongated terminal chambers in biserial morphotype of *P. hariaensis* and tubulospines in *P. hantkeninoides*.

Sixth, we observe a significant size reduction (close to 35%) of the tests of *Contusotruncana contusa* (Lilliput effect). Our biometric analyses indicate that the test sizes of *C. contusa* are around 1 mm-length before and after the LMWE interval. These test sizes are similar to those previously measured in samples by Kucera and Malmgren (1996) at Caravaca and El Kef samples for the terminal Cretaceous. However, Kucera and Malmgren (1996) analyzed only two samples from each site which were very close to the KPB, and therefore fail to catch the influence of LMWE, which prevents us from making a detailed comparison. Notwithstanding this issue, it is noteworthy that Kucera and Malmgren (1996) determined that largest sized tests of *C. contusa* come from the Caravaca and El Kef section and are around twice the size of those reported at higher latitudes sites. Although they did not perform biometric analysis, Keller and Abramovich (2009) provided examples of the Lilliput effect in late Maastrichtian planktic foraminifera and concluded that this was a response to a stressed environment. According to MacLeod et al. (2000), a smaller test size implies stunted growth and early sexual maturity, which maximizes survival rates in high-stress environments where survival depends on rapid turnover, as was the case for the LMWE.

Seventh, the increase of the fragmentation index (FI) during the LMWE indicates increased dissolution intensity and/or poor preservation of $CaCO_3$. One possible explanation can be a lysocline shoaling, but this seems unlikely due to the poor linear correlation between the P/B ratio and the FI (Fig. 10C). In addition, the P/B ratio remains stable along all the section, indicating no decline in planktic foraminiferal flux to the seafloor as the result of a rapid rise of the lysocline. The carbonate sediments of Caravaca were apparently deposited well above the foraminiferal lysocline, but FI indicates relatively poor preservation and high amounts of test dissolution in intervals from 15.60 to 10.80 m and 7.50 to 6.30 m below the KPB. This apparent contradiction between FI and P/B ratio could be explained by local surface water becoming more acidic, perhaps due to a short-lived increase in the atmospheric partial pressure of CO_2 (Henehan et al., 2016, 2019).

Although there are differences in absolute fragmentation index values between Caravaca and sites in the Pacific and South Atlantic (Fig. 14; Kucera et al., 1997; Henehan et al., 2016), a significant increase in fragmentation index can be observed close to the C30n/C29r boundary in all the localities, followed by relatively high values during the LMWE. In the last 100 kyr of the Maastrichtian, the fragmentation index seems to be more variable, but returned to values similar to the pre-LMWE interval, which is especially evident at Caravaca and DSDP 527. Other moderate to strong carbonate dissolution intervals broadly coeval with those identified in Fig. 14 have been also reported from South Atlantic DSDP Site 528 and Central Pacific DSDP Site 577 by D'Hondt (2005), albeit with a lower sampling resolution. According to the fragmentation records discussed here, it is suggested that widespread ocean acidification during the LMWE was probably linked to Deccan volcanism.

According to our data summarized in Fig. 15, the maximum in ecological stress, evidenced by the planktic foraminifera assemblages, occurred towards the end of the LMWE in the studied section. This event is recorded 6.55 m below the KTB and is characterized by the low values in $\delta^{18}O$ and $\delta^{13}C$, the highest relative abundance of *Heterohelix* (82.3%), the lowest relative abundance of globotruncanids (0%), and the lowest D/S ratio (0%) (see Supplementary Tables 2 and 4). Maximum FI values seem to concentrate in the LMWE, but they do not coincide precisely with the excursions of both $\delta^{18}O$ and $\delta^{13}C$.

In order to reduce the influence of the most extreme $\delta^{18}O$ and $\delta^{13}C$ values, smoothed curves were produced using the non-parametric Locally Weighted Scatterplot Smoothing (LOWESS; span = 0.3) and compared to the most relevant planktic foraminiferal proxies (Fig. 15). These smoothed records were generated both with and without the three 'extreme' values shown in Fig. 13

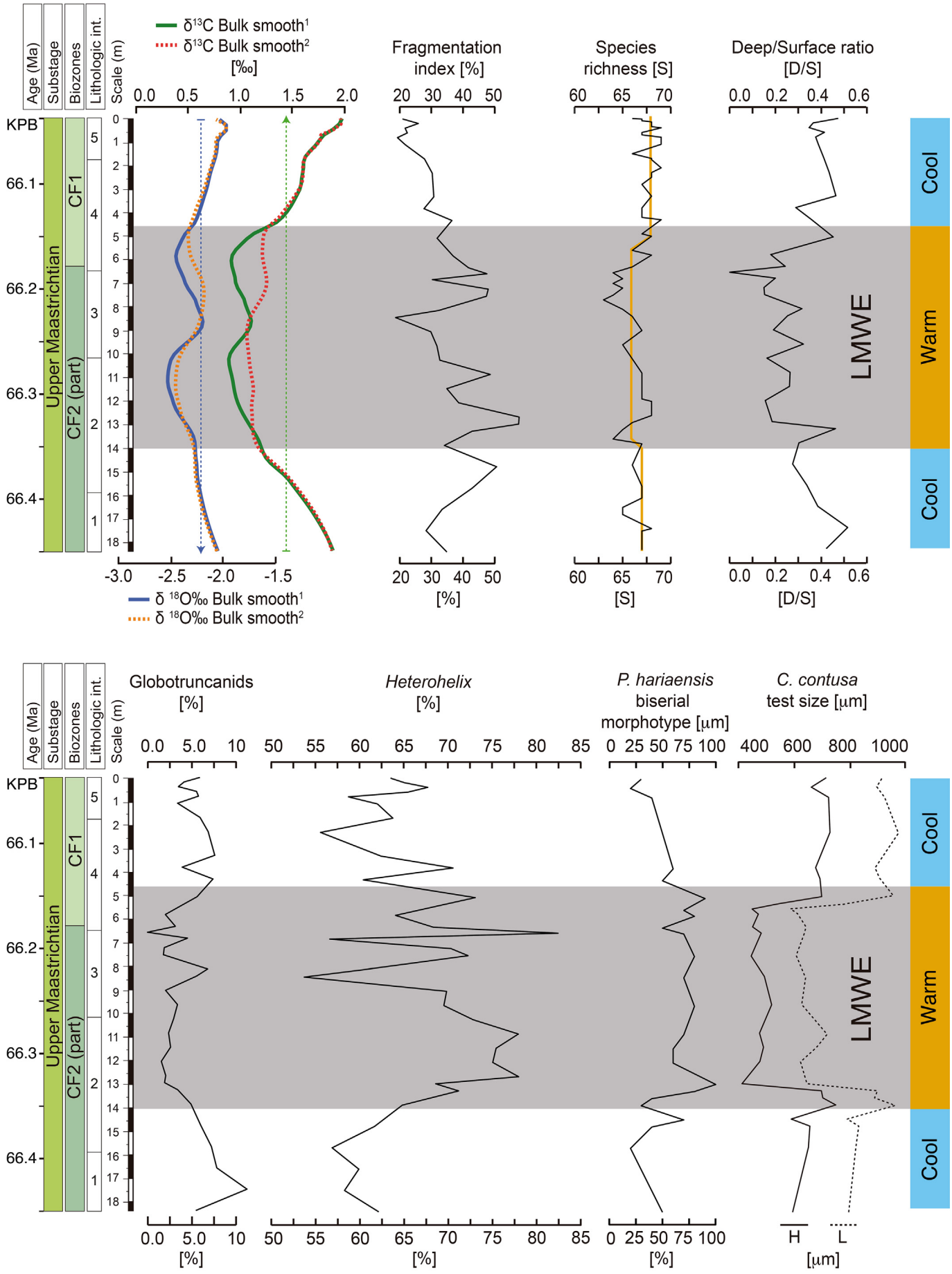

Fig. 15. Summary of the changes in most relevant planktic foraminiferal and geochemical proxies, and position of the LMWE in the Caravaca section. [1]Smoothing considering all the dataset, [2]Smoothing excluding three potential outliers discussed in Section 6.1.

(discussed in Section 6.1). Both approaches yield similar long-term trends but reduce the influence of the outlying datapoints. Both approaches exhibit two intervals of warming within the LMWE, although the timing of the younger interval is slightly shifted in the smoothed record that excludes the outlying data points. Overall, this comparison between isotopic and micropaleontological data supports the hypothesis that two warmer intervals could have occurred during the LMWE. Using the smoothed record that includes all the available data, the first warmer interval occurred between 66.32 and 66.26 Ma (i.e., between 280 and 220 kyr before the KPB) and the second between 66.19 and 66.15 Ma (i.e., between 150 and 110 kyr before the KPB). Both are characterized by maxima values of low oxygen tolerant genus *Heterohelix* and negative excursions of $\delta^{18}O$ and $\delta^{13}C$. The intermediate interval is characterized by higher $\delta^{18}O$ and $\delta^{13}C$ values, a decrease in *Heterohelix*, and an increase in the globotruncanids, *Rugoglobigerina* and *Pseudoguembelina*, reliably related to cooler pulses within the LMWE interval. Recently, Woelders et al. (2018) compared multiple palaeotemperature proxies (stable oxygen isotope, Mg/Ca and TEX_{86}) from the latest Maastrichtian of Bass River, New Jersey and, on this basis, proposed at least two warmer intervals within the LMWE (see Fig. 3 of Woelders et al., 2018). We suggest that these two intervals may correlate with those recognized in Caravaca.

8. Latest Maastrichtian cooling and return to pre-LMWE conditions

After the LMWE, a worldwide cooling is well documented at the end of Maastrichtian, from oceanic ODP/IODP sites (see Fig. 13) and outcrop sites in Seymour Island, Antarctica (Petersen et al., 2016), Argentina (Woelders et al., 2017), North America (Vellekoop et al., 2016; Woelders et al., 2018) and Tunisia (Thibault et al., 2016). The global temperature compilation of Hull et al. (2020) also shows that the climate cooled at this time, returning to pre-LMWE conditions. At Caravaca, this trend in cooling is evidenced by the increase in $\delta^{18}O$ values recorded in the uppermost ~4.5 m of the section, i.e. during the last ~100 kyr of the Maastrichtian according to our age model (Fig. 15) and is consistent with the global pattern. The progressive decline in the FI values during this same interval suggests that surface waters were less corrosive after the LMWE up to the KPB. This contradicts the hypothesis that a major pulse of Deccan volcanism caused the most harmful effects, such as rapid warming and ocean acidification, just before the KPB (e.g., Font et al., 2014, 2017; Punekar et al., 2014, 2016; Keller et al., 2016; Schoene et al., 2019). Conversely, our results are consistent with the hypothesis of Henehan et al. (2019) in which ocean pH was stable over the last 100 kyr of the Cretaceous.

Planktic foraminiferal assemblages suffered minor reorganization during the LMWE but following the event the ecological proxies suggest a return to conditions similar to the pre-LMWE (Fig. 15). According to our data, water column stratification was reestablished during the end-Maastrichtian cooling, as suggested by the increase in the abundance of thermocline dwellers, especially globotruncanids, and the increase in the Deep/Surface ratio (Fig. 15 and Table S2). Species richness remained very high during the climate cooling, reaching the highest average value in species richness of the entire Caravaca section. Nevertheless, four HOs of planktic foraminiferal species (6% of the total number of species) have been recorded in the last 50 cm below the KPB (Fig. 6). However, three of these species (*A. blowi, P. manuelensis,* and *Gita. falsocalcarata*) have been identified just below the KPB in some western Tethyan sections including Agost, Spain (Molina et al., 1998), Aïn Settara and El Kef, Tunisia (Arenillas et al., 2000a,b; Gallala, 2013), and Sidi Ziane and Djebel Zakhamoune, Algeria (Metsana-Oussaid et al., 2019). Therefore, the extinction rate before the KPB was probably as low as 1.5%, since only *A. cretacea* actually became extinct just before the KPB, as part of the background extinction. Our data from Caravaca support high evolutionary stability during the latest Maastrichtian, and, therefore, indicate that the catastrophic planktic foraminiferal mass extinction at the KPB was caused by the Chicxulub impact (see Arenillas et al., 2000a, b, 2006; Arz et al., 2000; Lowery et al., 2018) and not by gradual environmental degradation induced by Deccan forcing as has been proposed by Keller (1988), Keller et al. (2012) and Punekar et al. (2014), among others.

9. Conclusions

In this work, we performed high-resolution micropaleontological and geochemical analyses of the last ~400 kyr of the Cretaceous from Caravaca (Spain, western Tethys), for the first time demonstrating the Latest Maastrichtian Warming Event (LMWE) in this section. As a warming indicator, we used the $\delta^{18}O$ in bulk-rock to demonstrate the presence of a warm phase from ~66.35 to 66.14 Ma. Our data suggest that the LMWE at Caravaca included at least two shorter warming pulses marked by relatively lower $\delta^{18}O$ and $\delta^{13}C$ values, probably related to two massive and short periods of greenhouse gas injection during Deccan outgassing activity. Simultaneously with warming, high values of the fragmentation index (FI) of planktic foraminiferal tests are recorded, reaching significant values that exceed 40%; these values may be the result of changes in the carbonate saturation state of surface oceanic waters.

At Caravaca, planktic foraminiferal proxies suggest high-stress conditions (including warming, decreased water mass stratification and reduced oxygenation) during the LMWE, ending ~100 kyr before the Cretaceous/Paleogene boundary (KPB). Later, species richness and all ecological proxies return to values similar to the pre-LMWE interval.

At Caravaca, no evidence of a gradual mass extinction in planktic foraminifera has been recognized below the Ir-rich air-fall layer that is linked to the Chicxulub impact marking the KPB. Although the warming pulses of the LMWE are near the KPB and seem to have had global repercussions, our results indicate that the climate effects of greenhouse gas emissions linked to the Deccan volcanism were too weak to be an essential factor in the end-Cretaceous mass extinctions. Future work is needed to constrain the evidence of Deccan volcanism across the K/Pg boundary and its influence on the decline and posterior recovery of marine ecosystems in the early Danian. It is crucial to better know why the Deccan, one of the biggest igneous provinces in the history of Earth, apparently caused such a weak effect on marine ecosystems while other mass extinctions have been related to similar styles of large igneous province eruption.

Acknowledgments

We deeply thank the editor and two anonymous reviewers for their useful, comprehensive and helpful comments and suggestions. This work was supported by MCIU (Ministerio de Ciencia, Innovación y Universidades)/AEI (Agencia Estatal de Investigación)/FEDER (Fondo Europeo de Desarrollo Regional), UE (grant number PGC2018-093890-B-I00), and by the Aragonian Government/FEDER, UE (grant number DGA groups E33_17R and E33_20R). Vicente Gilabert acknowledges support from the Spanish Ministerio de Economía, Industria y Competitividad (FPI grant number BES-2016-077800). The authors would like to acknowledge the use of the Servicio General de Apoyo a la Investigación-SAI, Universidad de Zaragoza. This research is part of the PhD thesis of the first author.

References

Abramovich, S., Keller, G., 2002. High stress late Maastrichtian paleoenvironment: Inference from planktonic foraminifera in Tunisia. Palaeogeography, Palaeoclimatology, Palaeoecology 178, 145–164. https://doi.org/10.1016/S0031-0182(01)00394-7.

Abramovich, S., Keller, G., 2003. Planktonic foraminiferal response to the latest Maastrichtian abrupt warm event: a case study from South Atlantic DSDP Site 525A. Marine Micropaleontology 48, 225–249. https://doi.org/10.1016/S0377-8398(03)00021-5.

Abramovich, S., Keller, G., Stüben, D., Berner, Z., 2003. Characterization of late Campanian and Maastrichtian planktonic foraminiferal depth habitats and vital activities based on stable isotopes. Palaeogeography, Palaeoclimatology, Palaeoecology 202, 1–29. https://doi.org/10.1016/S0031-0182(03)00572-8.

Abramovich, S., Yovel-Corem, S., Almogi-Labin, A., Benjamini, C., 2010. Global climate change and planktic foraminiferal response in the Maastrichtian. Paleoceanography 25 (2), PA2201. https://doi.org/10.1029/2009PA001843.

Abramovich, S., Keller, G., Berner, Z., Cymbalista, M., Rak, C., 2011. Maastrichtian planktic foraminiferal biostratigraphy and paleoenvironment of Brazos River, Falls County, Texas. In: Keller, G., Adatte, T. (Eds.), The End-Cretaceous Mass Extinction and the Chicxulub Impact in Texas. Society for Sedimentary Geology Special Publication 100, pp. 123–156.

Alvarez, L.W., Alvarez, W., Asaro, F., Michel, H.V., 1980. Extraterrestrial Cause for the Cretaceous-Tertiary Extinction. Science 208, 1095–1108. https://doi.org/10.1126/science.208.4448.1095.

Andeweg, B., 2002. Cenozoic tectonic evolution of the Iberian Peninsula: effects and causes of changing stress fields. PhD thesis. Vrije Universiteit Amsterdam, Amsterdam, p. 192.

Arenillas, I., Arz, J.A., Molina, E., Dupuis, C., 2000a. The Cretaceous/Paleogene (K/P) boundary at Aïn Settara, Tunisia: sudden catastrophic mass extinction in planktic foraminifera. Journal of Foraminiferal Research 30, 202–218. https://doi.org/10.2113/0300202.

Arenillas, I., Arz, J.A., Molina, E., Dupuis, C., 2000b. An independent test of planktonic foraminiferal turnover across the Cretaceous/Paleogene (K/P) boundary at El Kef, Tunisia: Catastrophic mass extinction and possible survivorship. Micropaleontology 46, 31–49.

Arenillas, I., Arz, J.A., Grajales-Nishimura, J.M., Murillo-Muñetón, G., Alvarez, W., Camargo-Zanoguera, A., Molina, E., Rosales-Domínguez, C., 2006. Chicxulub impact event is Cretaceous/Paleogene boundary in age: new micropaleontological evidence. Earth and Planetary Science Letters 249, 241–257.

Arz, J.A., Arenillas, I., Molina, E., Sepulveda, R., 2000. La estabilidad evolutiva de los foraminíferos planctónicos en el Maastrichtiense Superior y su extinción en el límite Cretácico/Terciario de Caravaca, España. Revista Geologica de Chile 27, 27–47.

Ashckenazi-Polivoda, S., Rak, C., Almogi-Labin, A., Zsolt, B., Ovadia, O., Abramovich, S., 2014. Paleoecology of the K-Pg mass extinction survivor *Guembelitria* (Cushman): isotopic evidence from pristine foraminifera from Brazos River, Texas (Maastrichtian). Paleobiology 40, 24–33. https://doi.org/10.1666/13317.

Batenburg, S.J., Sprovieri, M., Gale, A.S., Hilgen, F.J., Hüsing, S., Laskar, J., Liebrand, D., Lirer, F., Orue-Etxebarria, X., Pelosi, N., Smit, J., 2012. Cyclostratigraphy and astronomical tuning of the Late Maastrichtian at Zumaia (Basque country, Northern Spain). Earth and Planetary Science Letters 359–360, 264–278. https://doi.org/10.1016/j.epsl.2012.09.054.

Batenburg, S.J., Friedrich, O., Moriya, K., Voigt, S., Cournède, C., Moebius, I., Blum, P., Bornemann, A., Fiebig, J., Hasegawa, T., Hull, P.M., Norris, R.D., Röhl, U., Sexton, P.F., Westerhold, T., Wilson, P.A., IODP Expedition Scientists, 2018. Late Maastrichtian carbon isotope stratigraphy and cyclostratigraphy of the Newfoundland Margin (Site U1403, IODP Leg 342). Newsletters on Stratigraphy 51 (2), 245–260. https://doi.org/10.1127/nos/2017/0398.

Barnet, J.S.K., Littler, K., Kroon, D., Leng, M.J., Westerhold, T., Röhl, U., Zachos, J.C., 2018. A new high-resolution chronology for the late Maastrichtian warming event: Establishing robust temporal links with the onset of Deccan volcanism. Geology 46 (2), 147–150. https://doi.org/10.1130/G39771.1.

Barnet, J.S.K., Littler, K., Westerhold, T., Kroon, D., Leng, M.J., Bailey, I., Röhl, U., Zachos, J.C., 2019. A High-Fidelity Benthic Stable Isotope Record of Late Cretaceous–Early Eocene Climate Change and Carbon-Cycling. Paleoceanography and Paleoclimatology 34, 672–691. https://doi.org/10.1029/2019PA003556.

Barrera, E., Savin, S.M., 1999. Evolution of late Campanian-Maastrichtian marine climates and oceans. In: Barrera, E., Johnson, C.C. (Eds.), Evolution of the Cretaceous Ocean-Climate System. Geological Society of America Special Paper 332, pp. 245–282.

Berger, W.H., Bonneau, M.C., Parker, F.L., 1982. Foraminifera on the deep-sea floor: lysocline and dissolution rate. Oceanologica Acta 5, 249–258, 0399-1784/1982/249.

BouDagher-Fadel, M.K., Banner, F.T., Whittaker, J.E., 1997. The Early evolutionary History of planktonic foraminifera. Chapman and Hall, New York, p. 269.

Canudo, J.I., 2018. The collection of type fossils of the Natural Science Museum of the University of Zaragoza (Spain). Geoheritage 10, 385–392. https://doi.org/10.1007/s12371-017-0228-1.

Canudo, J.I., Keller, G., Molina, E., 1991. Cretaceous/Tertiary boundary extinction pattern and faunal turnover at Agost and Caravaca, S.E. Spain. Marine Micropaleontology 17, 319–341. https://doi.org/10.1016/0377-8398(91)90019-3.

Chacón, B., 2002. Las sucesiones hemipelágicas del final del Cretácico e inicio del Paleógeno en el SE de la Placa Ibérica: Estratigrafía de eventos y evolución de la cuenca. PhD thesis. Universidad Complutense, Madrid, p. 440.

Chenet, A.L., Quidelleur, X., Fluteau, F., Courtillot, V., Bajpai, S., 2007. ^{40}K-^{40}Ar dating of the Main Deccan large igneous province: Further evidence of KTB age and short duration. Earth and Planetary Science Letters 263, 1–15. https://doi.org/10.1016/j.epsl.2007.07.011.

Chenet, A.L., Fluteau, F., Courtillot, V., Gérard, M., Subbarao, K.V., 2008. Determination of rapid Deccan eruptions across the Cretaceous-Tertiary boundary using paleomagnetic secular variation: Results from a 1200-m-thick section in the Mahabaleshwar escarpment. Journal of Geophysical Research Solid Earth 113. https://doi.org/10.1029/2006JB004635.

Chenet, A.L., Courtillot, V., Fluteau, F., Gérard, M., Quidelleur, X., Khadri, S.F.R., Subbarao, K.V., Thordarson, T., 2009. Determination of rapid Deccan eruptions across the Cretaceous-Tertiary boundary using paleomagnetic secular variation: 2. Constraints from analysis of eight new sections and synthesis for a 3500-m-thick composite section. Journal of Geophysical Research Solid Earth 114, 1–38. https://doi.org/10.1029/2008JB005644.

Clarke, L.J., Jenkyns, H.C., 1999. New oxygen isotope evidence for long-term Cretaceous climatic change in the Southern Hemisphere. Geology 27, 699–702.

Coccioni, R., Galeotti, S., 1994. K-T boundary extinction: Geologically instantaneous or gradual event? Evidence from deep-sea benthic foraminifera. Geology 22, 779–782. https://doi.org/10.1130/0091-7613(1994)022<0779:KTBEGI>2.3.CO;2.

Coccioni, R., Premoli Silva, I., 2015. Revised Upper Albian-Maastrichtian planktonic foraminiferal biostratigraphy and magneto-stratigraphy of the classical Tethyan Gubbio section (Italy). Newsletters on Stratigraphy 48, 47–90. https://doi.org/10.1127/nos/2015/0055.

Coccioni, R., Luciani, V., Marsili, A., 2006. Cretaceous oceanic anoxic events and radially elongated chambered planktonic foraminifera: Paleoecological and paleoceanographic implications. Palaeogeography, Palaeoclimatology, Palaeoecology 235, 66–92. https://doi.org/10.1016/j.palaeo.2005.09.024.

Courtillot, V., Fluteau, F., 2010. Cretaceous Extinctions: The volcanic hypothesis. Science 328, 973–974. https://10.1126/science.328.5981.975.

Dameron, S.N., Leckie, R.M., Clark, K., MacLeod, K.G., Thomas, D.J., Lees, J.A., 2017. Extinction, dissolution, and possible ocean acidification prior to the Cretaceous/Paleogene (K/Pg) boundary in the tropical Pacific. Palaeogeography, Palaeoclimatology, Palaeoecology 485, 433–454. https://doi.org/10.1016/j.palaeo.2017.06.032.

Dessert, C., Dupré, B., François, L.M., Schott, J., Gaillardet, J., Chakrapani, G., Bajpai, S., 2001. Erosion of Deccan Traps determined by river geochemistry: impact on the global climate and the 87Sr/86Sr ratio of seawater. Earth and Planetary Science Letters 188, 459–474. https://doi.org/10.1016/S0012-821X(01)00317-X.

D'Hondt, S., 2005. Consequences of the Cretaceous/Paleogene Mass Extinction for Marine Ecosystems. Annual Review of Ecology, Evolution, and Systematics 36, 295–317. https://doi.org/10.1146/annurev.ecolsys.35.021103.105715.

D'Hondt, S., Arthur, M.A., 1995. Interspecies variation in stable isotopic signals of Maastrichtian planktonic foraminifera. Paleoceanography 10, 123–135. https://doi.org/10.1029/94PA02671.

D'Hondt, S., Zachos, J.C., 1993. On stable isotopic variation and earliest Paleocene planktonic foraminifera. Paleoceanography 8, 527–547. https://doi.org/10.1029/93PA00952.

Falzoni, F., Petrizzo, M.R., Huber, B.T., MacLeod, K.G., 2014. Insights into the meridional ornamentation of the planktonic foraminiferal genus *Rugoglobigerina* (Late Cretaceous) and implications for taxonomy. Cretaceous Research 47, 87–104. https://doi.org/10.1016/j.cretres.2013.11.001.

Falzoni, F., Petrizzo, M.R., Clarke, L.J., MacLeod, K.G., Jenkyns, H.C., 2016. Long-term Late Cretaceous oxygen-and carbon isotope trends and planktonic foraminiferal turnover: A new record from the southern mid-latitudes. Bulletin of the Geological Society of America 128, 1725–1735. https://doi.org/10.1130/B31399.1.

Font, E., Fabre, S., Nédélec, A., Adatte, T., Keller, G., Veiga-Pires, C., Ponte, J., Mirão, J., Khozyem, H., Spangenberg, J.E., 2014. Atmospheric halogen and acid rains during the main phase of Deccan eruptions: magnetic and mineral evidence. In: Keller, G., Kerr, A.C. (Eds.), Volcanism, Impacts, and Mass Extinctions: Causes and Effects. Geological Society of America Special Paper 505, pp. 353–368. https://doi.org/10.1130/2014.2505(18).

Font, E., Adatte, T., Sial, A.N., Drude de Lacerda, L., Keller, G., Punekar, J., 2016. Mercury anomaly, Deccan volcanism, and the end-Cretaceous mass extinction. Geology 44, 171–174. https://doi.org/10.1130/G37451.1.

Font, E., Carlut, J., Rémazeilles, C., Mather, T.A., Nédélec, A., Mirão, J., Casale, S., 2017. End-Cretaceous akaganéite as a mineral marker of Deccan volcanism in the sedimentary record. Scientific Reports 7 (11453). https://doi.org/10.1038/s41598-017-11954-y.

Gallala, N., 2013. Planktonic Foraminiferal Biostratigraphy and Correlation Across the Cretaceous-Paleogene Transition at the Tethyan and the Atlantic Realms. Paleontology Journal 2013, 1–20. https://doi.org/10.1155/2013/643278.

Gradstein, F.M., Ogg, J.G., Schmitz, M., Ogg, G., 2012. The Geological Time Scale 2012. Elsevier Science Ltd., Boston, p. 1144. https://doi.org/10.1016/C2011-1-08249-8.

Georgescu, M.D., Saupe, E.E., Huber, B.T., 2008. Morphometric and stratophenetic basis for phylogeny and taxonomy in Late Cretaceous gublerinid planktonic foraminifera. Micropaleontology 54, 397–424.

Gertsch, B., Keller, G., Adatte, T., Garg, R., Prasad, V., Fleitmann, D., Berner, Z., 2011. Environmental effects of Deccan volcanism across the Cretaceous–Tertiary transition in Meghalaya, India. Earth and Planetary Science Letters 310, 272–285. https://doi.org/10.1016/j epsl.2011.08.015.

Helm, K.P., Bindoff, N.L., Church, J.A., 2011. Observed decreases in oxygen content of the global ocean: Global decreases in ocean oxygenic levels. Geophysical Research Letters 38, 1–6. https://doi.org/10.1029/2011GL049513.

Henehan, M.J., Hull, P.M., Penman, D.E., Rae, J.W.B., Schmidt, D.N., 2016. Biogeochemical significance of pelagic ecosystem function: an end-Cretaceous case study. Philosophical Transactions of the Royal Society B: Biological Sciences 371 (20150510). https://doi.org/10.1098/rstb.2015.0510.

Henehan, M.J., Ridgwell, A., Thomas, E., Zhang, S., Alegret, L., Schmidt, D.N., Rae, J.W.B., Witts, J.D., Landman, N.H., Greene, S.E., Huber, B.T., Super, J.R., Planavsky, N.J., Hull, P.M., 2019. Rapid ocean acidification and protracted Earth system recovery followed the end-Cretaceous Chicxulub impact. Proceedings of the National Academy of Sciences of the United States of America 116, 22500–22504. https://doi.org/10.1073/pnas.1905989116.

Huber, B.T., Hodell, D.A., Hamilton, C.P., 1995. Middle–Late Cretaceous climate of the southern high latitudes: Stable isotopic evidence for minimal equator-to-pole thermal gradients. The Geological Society of America Bulletin 107 (10), 1164–1191. https://doi.org/10.1130/0016-7606(1995)107<1164:MLCCOT>2.3.CO;2.

Huber, B.T., MacLeod, K.G., Watkins, D.K., Coffin, M.F., 2018. The rise and fall of the Cretaceous Hot Greenhouse climate. Global and Planetary Change 167, 1–23. https://doi.org/10.1016/j.gloplacha.2018.04.004.

Hull, P.M., Bornemann, A., Penman, D.E., Henehan, M.J., Norris, R.D., Wilson, P.A., Blum, P., Alegret, L., Batenburg, S.J., Bown, P.R., Bralower, T.J., Cournede, C., Deutsch, A., Donner, B., Friedrich, O., Jehle, S., Kim, H., Kroon, D., Lippert, P.C., Loroch, D., Moebius, I., Moriya, K., Peppe, D.J., Ravizza, G.E., Röhl, U., Schueth, J.D., Sepúlveda, J., Sexton, P.F., Sibert, E.C., Śliwińska, K.K., Summons, R.E., Thomas, E., Westerhold, T., Whiteside, J.H., Yamaguchi, T., Zachos, J.C., 2020. On impact and volcanism across the Cretaceous-Paleogene boundary. Science 367, 266–272. https://doi.org/10.1126/science.aay5055.

Husson, D., Galbrun, B., Gardin, S., Thibault, N., 2014. Tempo and duration of short-term environmental perturbations across the Cretaceous-Paleogene boundary. Stratigraphy 11, 159–171. https://hal.archives-ouvertes.fr/hal-01092775.

Isaza-Londoño, C., MacLeod, K.G., Huber, B.T., 2006. Maastrichtian North Atlantic warming, increasing stratification, and foraminiferal paleobiology at three timescales. Paleoceanography 21, 1–10. https://doi.org/10.1029/2004PA001130.

Jarvis, I., Gale, A.S., Jenkyns, H.C., Pearce, M.A., 2006. Secular variation in Late Cretaceous carbon isotopes: a new δ13C carbonate reference curve for the Cenomanian – Campanian (99.6–70.6 Ma). Geological Magazine 143, 561–608. https://doi.org/10.1017/S0016756806002421.

Jenkyns, H.C., Gale, A.S., Corfield, R.M., 1994. Carbon- and oxygen-isotope stratigraphy of the English Chalk and Italian Scaglia and its palaeoclimatic significance. GeoLogical Magazine 131, 1–34. https://doi.org/10.1017/S0016756800010451.

Kaiho, K., Lamolda, M.A., 1999. Catastrophic extinction of planktonic foraminifera at the Cretaceous-Tertiary boundary evidenced by stable isotopes and foraminiferal abundance at Caravaca, Spain. Geology 27, 355–358. https://doi.org/10.1130/0091-7613(1999)027<0355:CEOPFA>2.3.CO;2.

Keller, G., 1988. Extinctions, Survivorship and Evolution across the Cretaceous/Tertiary Boundary at El Kef, Tunisia. Marine Micropaleontology 13, 239–263. https://doi.org/10.1016/0377-8398(88) 90005–90009.

Keller, G., 2014. Deccan volcanism, the Chicxulub impact, and the end-Cretaceous mass extinction: Coincidence? Cause and effect? In: Keller, G., Kerr, A.C. (Eds.), Volcanism, Impacts, and Mass Extinctions: Causes and Effects. Geological Society of America Special Paper 505, pp. 57–89. https://doi.org/10.1130/2014.2505(03).

Keller, G., Abramovich, S., 2009. Lilliput effect in late Maastrichtian planktic foraminifera: Response to environmental stress. Palaeogeography, Palaeoclimatology, Palaeoecology 284, 47–62. https://doi.org/10.1016/j.palaeo.2009.08.029.

Keller, G., Adatte, T., Gardin, S., Bartolini, A., Bajpai, S., 2008. Main Deccan volcanism phase ends near the K-T boundary: evidence from the Krishna-Godavari Basin, SE India. Earth and Planetary Science Letters 268, 293–311. https://doi.org/10.1016/j.epsl.2008.01.015.

Keller, G., Adatte, T., Pardo, A., Bajpal, S., Khosla, A., Samant, B., 2010. Cretaceous Extinctions: Evidence Overlooked. Science 328, 974–975. https://10.1126/science.328.5981.975.

Keller, G., Adatte, T., Bhowmick, P., Upadhyay, H., Dave, A., Reddy, A.N., Jaiprakash, B.C., 2012. Nature and timing of extinctions in Cretaceous-Tertiary planktic foraminifera preserved in Deccan intertrappean sediments of the Krishna–Godavari Basin, India. Earth and Planetary Science Letters 341–344, 211–221. https://doi.org/10.1016/j.epsl.2012.06.021.

Keller, G., Punekar, J., Mateo, P., 2016. Upheavals during the Late Maastrichtian: Volcanism, climate and faunal events preceding the end-Cretaceous mass extinction. Palaeogeography, Palaeoclimatology, Palaeoecology 441, 137–151. https://doi.org/10.1016/j.palaeo.2015.06.034.

Kring, D.A., 2007. The Chicxulub impact event and its environmental consequences at the Cretaceous–Tertiary boundary. Palaeogeography, Palaeoclimatology, Palaeoecology 255, 4–21. https://doi.org/10.1016/j.palaeo.2007.02.037.

Kucera, M., Malmgren, B.A., 1996. Latitudinal variation in the planktic foraminifer *Contusotruncana contusa* in the terminal Cretaceous ocean. Marine Micropaleontology 28, 31–52. https://doi.org/10.1016/0377-8398(95)00078-X.

Kucera, M., Malmgren, B.A., Sturesson, U., 1997. Foraminiferal dissolution at shallow depths of the Walvis Ridge and Rio Grande Rise during the latest Cretaceous: Inferences for deep-water circulation in the South Atlantic. Palaeogeography, Palaeoclimatology, Palaeoecology 129, 195–212. https://doi.org/10.1016/S0031-0182(96)00133-2.

Li, L., Keller, G., 1998a. Abrupt deep-sea warming at the end of the Cretaceous. Geology 26, 995–998. https://doi.org/10.1130/0091-7613(1998)026<0995:ADSWAT>2.3.CO;2.

Li, L., Keller, G., 1998b. Diversification and extinction in Campanian-Maastrichtian planktic foraminifera of Northwestern Tunisia. Eclogae Geologicae Helvetiae 91, 75–102.

Linnert, C., Robinson, S.A., Lees, J.A., Bown, P.R., Rodríguez, I.P., Petrizzo, M.R., Falzoni, F., Littler, K., Arz, J.A., Russell, E.E., 2014. Evidence for global cooling in the Late Cretaceous. Nature Communications 5, 4194. https://doi.org/10.1038/ncomms5194.

Lowery, C.M., Bralower, T.J., Owens, J.D., Rodríguez-Tovar, F.J., Jones, H., Smit, J., Whalen, M.T., Claeys, P., Farley, K., Gulick, S.P.S., Morgan, J.V., Green, S., Chenot, E., Christeson, G.L., Cockell, C.S., Coolen, M.J.L., Ferrière, L., Gebhardt, C., Goto, K., Kring, D.A., Lofi, J., Ocampo-Torres, R., Perez-Cruz, L., Pickersgill, A.E., Poelchau, M.H., Rae, A.S.P., Rasmussen, C., Rebolledo-Vieyra, M., Riller, U., Sato, H., Tikoo, S.M., Tomioka, N., Urrutia-Fucugauchi, J., Vellekoop, J., Wittmann, A., Xiao, L., Yamaguchi, K.E., Zylberman, W., 2018. Rapid recovery of life at ground zero of the end-Cretaceous mass extinction. Nature 558, 288–291. https://doi.org/10.1038/s41586-018-0163-6.

Luciani, V., Giusberti, L., Agnini, C., Backman, J., Fornaciari, E., Rio, D., 2007. The Paleocene–Eocene Thermal Maximum as recorded by Tethyan planktonic foraminifera in the Forada section (northern Italy). Marine Micropaleontology 64, 189–214. https://doi.org/10.1016/j.marmicro.2007.05.001.

MacLeod, N., Ortiz, N., Fefferman, N., Clyde, W., Schulter, C., MacLean, J., 2000. Phenotypic response of foraminifera to episodes of global environmental change. In: Culver, S.J., Rawson, P. (Eds.), Biotic Response to Global Environmental Change: The Last 145 Million Years. Cambridge University Press, Cambridge, pp. 51–78. https://doi.org/10.1017/CBO9780511535505.006.

MacLeod, K.G., Huber, B.T., Isaza-Londoño, C., 2005. North Atlantic warming during global cooling at the end of the Cretaceous. Geology 33, 437–440. https://doi.org/10.1130/G21466.1.

Malmgren, B.A., 1987. Differential dissolution of Upper Cretaceous planktonic foraminifera from a temperate region of the South Atlantic Ocean. Marine Micropaleontology 11, 251–271. https://doi.org/10.1016/0377-8398(87)90001-6.

Metsana-Oussaid, F., Belhai, D., Arenillas, I., Arz, J.A., Gilabert, V., 2019. New sections of the Cretaceous–Paleogene transition in the southwestern Tethys (Médéa, northern Algeria): planktic foraminiferal biostratigraphy and biochronology. Arabian Journal of Geosciences 12. https://doi.org/10.1007/s12517-019-4402-4.

Molina, E., Arenillas, I., Arz, J.A., 1998. Mass extinction in planktic foraminifera at the Cretaceous/Tertiary boundary in subtropical and temperate latitudes. Bulletin de la Societe Geologique de France 169, 351–363.

Molina, E., Alegret, L., Arenillas, I., Arz, J.A., Gallala, N., Grajales-Nishimura, M., Murillo-Muñetón, G., Zaghbib-Turki, D., 2009. The Global Boundary Stratotype Section and Point for the base of the Danian Stage (Paleocene, Paleogene, "Tertiary", Cenozoic): auxiliary sections and correlation. Episodes 32 (2), 84–95. https://doi.org/10.18814/epiiugs/2009/v32i2/002.

Nordt, L., Atchley, S., Dworkin, S., 2003. Terrestrial evidence for two greenhouse events in the latest Cretaceous. Geological Society of America Today 13, 4–9. https://doi.org/10.1130/1052-5173(2003)013<4:TEFTGE>2.0.CO;2.

O'Brien, C.L., Robinson, S.A., Pancost, R.D., Sinninghe Damsté, J.S., Schouten, S., Lunt, D.J., Alsenz, H., Bornemann, A., Bottini, C., Brassell, S.C., Farnsworth, A., Forster, A., Huber, B.T., Inglis, G.N., Jenkyns, H.C., Linnert, C., Littler, K., Markwick, P., McAnena, A., Mutterlose, J., Naafs, B.D.A., Püttmann, W., Sluijs, A., van Helmond, N.A.G.M., Vellekoop, J., Wagner, T., Wrobel, N.E., 2017. Cretaceous sea-surface temperature evolution: Constraints from TEX86 and planktonic foraminiferal oxygen isotopes. Earth-Science Reviews 172, 224–247. https://doi.org/10.1016/j.earscirev.2017.07.012.

O'Connor, L.K., Robinson, S.A., Naafs, B.D.A., Jenkyns, H.C., Henson, S., Clarke, M., Pancost, R.D., 2019. Late Cretaceous Temperature Evolution of the Southern High Latitudes: A TEX86 Perspective. Paleoceanography and Paleoclimatology 34, 436–454. https://doi.org/10.1029/2018PA003546.

Pardo, A., Keller, G., 2008. Biotic effects of environmental catastrophes at the end of the Cretaceous and early Tertiary: *Guembelitria* and *Heterohelix* blooms. Cretaceous Research 29, 1058–1073. https://doi.org/10.1016/j.cretres.2008.05.031.

Petersen, S.V., Dutton, A., Lohmann, K.C., 2016. End-Cretaceous extinction in Antarctica linked to both Deccan volcanism and meteorite impact via climate change. Nature Communications 7, 12079. https://doi.org/10.1038/ncomms12079.

Petrizzo, M.R., Huber, B.T., Falzoni, F., MacLeod, K.G., 2020. Changes in biogeographic distribution patterns of southern mid-to high latitude planktonic foraminifera during the Late Cretaceous hot to cool greenhouse climate transition. Cretaceous Research 115 (104547). https://doi.org/10.1016/j.cretres.2020.104547.

Percival, L., Jenkyns, H.C., Mather, T.A., Dickson, A.J., Batenburg, S.J., Ruhl, M., Hesselbo, S.P., Barclay, R., Jarvis, I., Robinson, S.A., Woelders, L., 2018. Does large igneous province volcanism always perturb the mercury cycle? Comparing the records of Oceanic Anoxic Event 2 and the end-Cretaceous to other Mesozoic events. American Journal of Science 318, 799–860. https://doi.org/10.2475/08.2018.01.

Premoli Silva, I., Sliter, W.V., 1999. Cretaceous paleoceanography: evidence from planktonic foraminiferal evolution. In: Barrera, E., Johnson, C.C. (Eds.), Evolution of the Cretaceous Ocean-Climate System. Geological Society of America Special Paper 332, pp. 301–328. https://doi.org/10.1130/0-8137-2332-9.301.

Punekar, J., Mateo, P., Keller, G., 2014. Environmental and biological effects of Deccan volcanism: a global survey. In: Keller, G., Kerr, A.C. (Eds.), Volcanism, Impacts, and Mass Extinctions: Causes and Effects. Geological Society of America Special Paper 505, pp. 91–116. https://doi.org/10.1130/2014.2505(04).

Punekar, J., Keller, G., Khozyem, H.M., Adatte, T., Font, E., Spangenberg, J., 2016. A multi-proxy approach to decode the end-Cretaceous mass extinction. Palaeogeography, Palaeoclimatology, Palaeoecology 441, 116–136. https://doi.org/10.1016/j.palaeo.2015.08.025.

Renne, P.R., Deino, A.L., Hilgen, F.J., Kuiper, K.F., Mark, D.F., Mitchell, W.S., Morgan, L.E., Mundil, R., Smit, J., 2013. Time scales of critical events around the Cretaceous-Paleogene boundary. Science 339, 684–687. https://doi.org/10.1126/science.1230492.

Renne, P.R., Sprain, C.J., Richards, M.A., Self, S., Vanderkluysen, L., Pande, K., 2015. State shift in Deccan volcanism at the Cretaceous-Paleogene boundary, possibly induced by impact. Science 350, 76–78. https://doi.org/10.1126/science.aac7549.

Robinson, N., Ravizza, G., Coccioni, R., Peucker-Ehrenbrink, B., Norris, R., 2009. A high-resolution marine $^{187}Os/^{188}Os$ record for the late Maastrichtian: Distinguishing the chemical fingerprints of Deccan volcanism and the KP impact event. Earth and Planetary Science Letters 281, 159–168. https://doi.org/10.1016/j.epsl.2009.02.019.

Schoene, B., Samperton, K.M., Eddy, M.P., Keller, G., Adatte, T., Bowring, S.A., Khadri, S.F.R., Gertsch, B., 2015. U-Pb geochronology of the Deccan Traps and relation to the end-Cretaceous mass extinction. Science 347, 182–184. https://doi.org/10.1126/science.aaa0118.

Schoene, B., Eddy, M.P., Samperton, K.M., Keller, C.B., Keller, G., Adatte, T., Khadri, S.F.R., 2019. U-Pb constraints on pulsed eruption of the Deccan Traps across the end-Cretaceous mass extinction. Science 363, 862–866. https://doi.org/10.1126/science.aau2422.

Scholle, P.A., Arthur, M.A., 1980. Carbon isotope fluctuations in Cretaceous pelagic limestones: potential stratigraphic and petroleum exploration tool. American Association of Petroleum Geologists Bulletin 64 (1), 67–87.

Schulte, P., Alegret, L., Arenillas, I., Arz, J.A., Barton, P.J., Bown, P.R., Bralower, T.J., Christeson, G.L., Claeys, P., Cockell, C.S., Collins, G.S., Deutsch, A., Goldin, T.J., Goto, K., Grajales-Nishimura, J.M., Grieve, R.A.F., Gulick, S.P.S., Johnson, K.R., Kiessling, W., Koeberl, C., Kring, D.A., MacLeod, K.G., Matsui, T., Melosh, J., Montanari, A., Morgan, J.V., Neal, C.R., Nichols, D.J., Norris, R.D., Pierazzo, E., Ravizza, G., Rebolledo-Vieyra, M., Reimold, W.U., Robin, E., Salge, T., Speijer, R.P., Sweet, A.R., Urrutia-Fucugauchi, J., Vajda, V., Whalen, M.T., Willumsen, P.S., 2010a. The Chicxulub asteroid impact and mass extinction at the Cretaceous-Paleogene boundary. Science 327, 1214–1218. https://doi.org/10.1126/science.1177265.

Schulte, P., Alegret, L., Arenillas, I., Arz, J.A., Barton, P.J., Bown, P.R., Bralower, T.J., Christeson, G.L., Claeys, P., Cockell, C.S., Collins, G.S., Deutsch, A., Goldin, T.J., Goto, K., Grajales-Nishimura, J.M., Grieve, R.A.F., Gulick, S.P.S., Johnson, K.R., Kiessling, W., Koeberl, C., Kring, D.A., MacLeod, K.G., Matsui, T., Melosh, J., Montanari, A., Morgan, J.V., Neal, C.R., D.J., Norris, R.D., Pierazzo, E., Ravizza, G., Rebolledo-Vieyra, M., Reimold, W.U., Robin, E., Salge, T., Speijer, R.P., Sweet, A.R., Urrutia-Fucugauchi, J., Vajda, V., Whalen, M.T., Willumsen, P.S., 2010b. Response – Cretaceous extinctions. Science 328, 975–976. https://10.1126/science.328.5981.975.

Sial, A.N., Chen, J., Lacerda, L.D., Frei, R., Tewari, V.C., Pandit, M.K., Gaucher, C., Ferreira, V.P., Cirilli, S., Peralta, S., Korte, C., Barbosa, J.A., Pereira, N.S., 2016. Mercury enrichment and Hg isotopes in Cretaceous–Paleogene boundary successions: Links to volcanism and palaeoenvironmental impacts. Cretaceous Research 66, 60–81. https://doi.org/10.1016/j.cretres.2016.05.006.

Signor, P.W., Lipps, J.H., 1982. Sampling bias, gradual extinction patterns and catastrophes in the fossil record. Geological Society of America Special Paper 190, 291–296. https://doi.org/10.1130/SPE190-p291.

Smit, J., 1982. Extinction and evolution of planktonic foraminifera after a major impact at the Cretaceous/Tertiary boundary. Geological Society of America Special Paper 190, 329–352. https://doi.org/10.1130/SPE190-p329.

Smit, J., 2004. The section of the Barranco del Gredero (Caravaca, SE Spain): a crucial section for the Cretaceous/Tertiary boundary impact extinction hypothesis. Journal of Iberian Geology 31, 179–191. https://doi.org/10.5209/JIGE.33967.

Smit, J., Klaver, G., 1981. Sanidine spherules indicate a large impact event. Nature 292, 47–49. https://doi.org/10.1038/292047a0.

Smit, J., ten Kate, W.G.H.Z., 1982. Trace-element patterns at the Cretaceous-Tertiary boundary - Consequences of a large impact. Cretaceous Research 3, 307–332. https://doi.org/10.1016/0195-6671(82)90031-3.

Sprain, C.J., Renne, P.R., Vanderkluysen, L., Pande, K., Self, S., Mittal, T., 2019. The eruptive tempo of Deccan volcanism in relation to the Cretaceous-Paleogene boundary. Science 363, 866–870. https://doi.org/10.1126/science.aav1446.

Sosa-Montes de Oca, C., Rodríguez-Tovar, F.J., Martínez-Ruiz, F., 2016. Geochemical and isotopic characterization of trace fossil infillings: New insights on trace-maker activity after the K/Pg impact event. Cretaceous Research 57, 391–401. https://doi.org/10.1016/j.cretres.2015.03.003.

Stott, L.D., Kennett, J.P., 1990. The paleoceanographic and paleoclimatic signature of the Cretaceous/Paleogene boundary in the Antarctic: stable isotopic results from ODP Leg 113, In: Proceedings of the Ocean Drilling Program. Scientific Results 113, 829–848. https://doi.org/10.2973/odp.proc.sr.113.158.1990.

Thibault, N., Gardin, S., 2010. The calcareous nannofossil response to the end-Cretaceous warm event in the Tropical Pacific. Palaeogeography, Palaeoclimatology, Palaeoecology 291, 239–252. https://doi.org/10.1016/j.palaeo.2010.02.036.

Thibault, N., Galbrun, B., Gardin, S., Minoletti, F., Le Callonnec, L.L., 2016. The end-Cretaceous in the southwestern Tethys (Elles, Tunisia): orbital calibration of paleoenvironmental events before the mass extinction. International Journal of Earth Sciences (Geologische Rundschau) 105, 771–795. https://doi.org/10.1007/s00531-015-1192-0.

Tobin, T.S., Ward, P.D., Steig, E.J., Olivero, E.B., Hilburn, I.A., Mitchell, R.N., Diamond, M.R., Raub, T.D., Kirschvink, J.L., 2012. Extinction patterns, $\delta^{18}O$ trends, and magnetostratigraphy from a southern high-latitude Cretaceous–Paleogene section: Links with Deccan volcanism. Palaeogeography, Palaeoclimatology, Palaeoecology 350–352, 180–188. https://doi.org/10.1016/j.palaeo.2012.06.029.

Vellekoop, J., Esmeray-Senlet, S., Miller, K.G., Browning, J.V., Sluijs, A., van de Schoot- brugge, B., Sinninghe Damsté, J.S., Brinkhuis, H., 2016. Evidence for Cretaceous– Paleogene boundary bolide "impact winter" conditions from New Jersey, USA. Geology 44, 619–622. https://doi.org/10.1130/G37961.1.

Vellekoop, J., Woelders, L., Sluijs, A., Miller, K.G., Speijer, R.P., 2019. Phytoplankton community disruption caused by latest Cretaceous global warming. Biogeosciences 16, 4201–4210. https://doi.org/10.5194/bg-16-4201-2019.

Voigt, S., Gale, A.S., Jung, C., Jenkyns, H.C., 2012. Global correlation of upper Campanian–Maastrichtian successions using carbon-isotope stratigraphy: Development of a new Maastrichtian timescale. Newsletters on Stratigraphy 45, 25–53. https://doi.org/10.1127/0078-0421/2012/0016.

Westerhold, T., Röhl, U., Donner, B., Mccarren, H.K., Zachos, J.C., 2011. A complete high-resolution Paleocene benthic stable isotope record for the central Pacific (ODP Site 1209). Paleoceanography 26, 1–13. https://doi.org/10.1029/2010PA002092.

Wilf, P., Johnson, K.R., Huber, B.T., 2003. Correlated terrestrial and marine evidence for global climate changes before mass extinction at the Cretaceous-Paleogene boundary. Proceedings of the National Academy of Sciences 100, 599–604. https://doi.org/10.1073/pnas.0234701100.

Woelders, L., Vellekoop, J., Kroon, D., Smit, J., Casadío, S., Prámparo, M.B., Dinarès-Turell, J., Peterse, F., Sluijs, A., Lenaerts, J.T.M., Speijer, R.P., 2017. Latest Cretaceous climatic and environmental change in the South Atlantic region. Paleoceanography 32. https://doi.org/10.1002/2016PA00300703007, 2016PA003007.

Woelders, L., Vellekoop, J., Weltje, G.J., de Nooijer, L., Reichart, G.-J., Peterse, F., Claeys, P., Speijer, R.P., 2018. Robust multi-proxy data integration, using late Cretaceous paleotemperature records as a case study. Earth and Planetary Science Letters 500, 215–224. https://doi.org/10.1016/j.epsl.2018.08.010.

Zhang, L., Wang, C., Wignall, P.B., Kluge, T., Wan, X., Wang, Q., Gao, Y., 2018. Deccan volcanism caused coupled pCO2 and terrestrial temperature rises, and pre-impact extinctions in northern China. Geology 46, 271–274. https://doi.org/10.1130/G39992.1.

Appendix A. Supplementary data

Supplementary data to this article can be found online at https://doi.org/10.1016/j.cretres.2021.104844.

Appendix. Alphabetic list of all species mentioned in the paper

Abathomphalus intermedius (Bolli, 1951).
Abathomphalus mayaroensis (Bolli, 1951).
Archaeoglobigerina blowi Pessagno, 1967.
Archaeoglobigerina cretacea (d'Orbigny, 1840).
Contusotruncana contusa (Cushman, 1926).
Contusotruncana patelliformis (Gandolfi, 1955).
Contusotruncana plicata (White, 1928).
Contusotruncana walfischensis (Todd, 1970).
Globigerinelloides multispina (Lalicker, 1948).
Globigerinelloides praeriehillensis (Pessagno, 1967).
Globigerinelloides rosebudensis Smith and Pessagno, 1973.
Globigerinelloides subcarinatus (Brönnimann, 1952).
Globigerinelloides volutus (White, 1928).
Globigerinelloides yaucoensis (Pessagno, 1960).
Globotruncana aegyptiaca Nakkady, 1950.
Globotruncana arca (Cushman, 1926).
Globotruncana mariei Banner and Blow, 1960.
Globotruncana orientalis El Naggar, 1966.
Globotruncana rosetta (Carsey, 1926).
Globotruncanella caravacaensis Smit, 1982.
Globotruncanella havanensis (Voorwijk, 1937).
Globotruncanella minuta Caron and González Donoso, 1984.
Globotruncanella petaloidea (Gandolfi, 1955).
Globotruncanella pschadae (Keller, 1946).
Globotruncanita angulata (Tilev, 1951).
Globotruncanita conica (White, 1928).
Globotruncanita dupeublei (Caron, González Donoso, Robaszynski and Wonders, 1984).
Globotruncanita falsocalcarata (Kerdany and Abdelsalam, 1969).
Globotruncanita fareedi (El Naggar, 1966).

Globotruncanita insignis (Gandolfi, 1955).
Globotruncanita stuarti (de Lapparent, 1918).
Globotruncanita stuartiformis (Dalbiez, 1955).
Gublerina acuta de Klasz, 1953.
Gublerina cuvillieri Kikoine, 1948.
Guembelitria blowi Arz, Arenillas and Náñez, 2010.
Guembelitria cretacea Cushman, 1933.
Heterohelix globulosa (Ehrenberg, 1840).
Heterohelix labellosa Nederbragt, 1991.
Heterohelix navarroensis Loeblich, 1951.
Heterohelix punctulata (Cushman, 1938).
Laeviheterohelix glabrans (Cushman, 1938).
Laeviheterohelix pulchra (Brotzen, 1936).
Muricohedbergella holmdelensis (Olsson, 1964).
Muricohedbergella monmouthensis (Olsson, 1960).
Planoglobulina acervulinoides (Egger, 1899).
Planoglobulina carseyae (Plummer, 1931).
Planoglobulina manuelensis (Martin, 1972).
Planoglobulina multicamerata (de Klasz, 1953).
Plummerita hantkeninoides (Brönnimann, 1952).
Pseudoguembelina costellifera Masters, 1976.
Pseudoguembelina costulata (Cushman, 1938).
Pseudoguembelina excolata (Cushman, 1926).
Pseudoguembelina hariaensis Nederbragt, 1991.
Pseudoguembelina kempensis Esker, 1968.
Pseudoguembelina palpebra Brönnimann and Brown, 1953.
Pseudotextularia elegans (Rzehak, 1891).
Pseudotextularia intermedia de Klasz, 1953.
Pseudotextularia nuttalli (Voorwijk, 1937).
Racemiguembelina fructicosa (Egger, 1899).
Racemiguembelina powelli Smith y Pessagno, 1973.
Rugoglobigerina hexacamerata Brönnimann, 1952.
Rugoglobigerina macrocephala Brönnimann, 1952.
Rugoglobigerina milamensis Smith and Pessagno, 1973.
Rugoglobigerina pennyi Brönnimann, 1952.
Rugoglobigerina reicheli Brönnimann, 1952.
Rugoglobigerina rotundata Brönnimann, 1952.
Rugoglobigerina rugosa (Plumier, 1926).
Rugoglobigerina scotti (Brönnimann, 1952).